Reviews in Mineralogy & Geochemistry
Vol. 75 pp. 251-287, 2013

Carbon in Silicate Melts

Huaiwei Ni and Hans Keppler

Bayerisches Geoinstitut
95440 Bayreuth, Germany

Hans.Keppler@uni-bayreuth.de

INTRODUCTION

Silicate melts are the main agent for transporting carbon from Earth's interior to the surface. The carbon concentration in the atmosphere and the size of the carbon reservoir in oceans, sediments, and biomass are ultimately controlled by the balance between carbon removal through weathering, burial in sediments, and subduction on one hand and volcanic degassing on the other hand (e.g., Berner 1994). Carbon emissions from volcanoes may have ended the Neoproterozoic "snowball-Earth" glaciation (Hoffman et al. 1998) and they have been invoked as a potential mechanism that could link flood basalt eruptions to mass extinction events (Beerling 2002).

In Earth's deep interior, the strong partitioning of carbon into silicate melts relative to solid minerals may contribute to melting in the seismic low-velocity zone of the upper mantle and in the transition zone (e.g., Dasgupta and Hirschmann 2010; Keshav et al. 2011). The formation of some highly silica-undersaturated melts is likely related to the effects of carbon dioxide on melting in the mantle (Brey and Green 1975). While carbon is usually less abundant than water in magmas erupting at Earth's surface, the lower solubility of carbon dioxide (either molecular or as CO_3^{2-}) in silicate melts implies that it is primarily carbon dioxide that controls the nucleation of bubbles, which is an important aspect of eruption dynamics (e.g., Holloway 1976; Papale and Polacci 1999). In the lower mantle, more reduced carbon species may be dominant in silicate melts, which may behave in a different way than carbon dioxide (e.g., Kadik et al. 2004). Data on the solubility and speciation of carbon in silicate melts (in a broad sense, covering superliquidus liquids, supercooled liquids and glasses) and its effect on melt properties are therefore essential for understanding a wide range of phenomena in the Earth system.

CARBON SOLUBILITY IN SILICATE MELTS

Under typical redox conditions in the present crust and upper mantle (ΔQFM ranging from −2 to +5; Wood et al. 1990; McCammon 2005) and the intrinsic conditions in experimental pressure vessels (generally above QFM; e.g., Jakobsson 1997; Tamic et al. 2001), thermodynamic calculations reveal that the majority of carbon is present as carbon dioxide in geological fluids (Pawley et al. 1992; Holloway and Blank 1994; Manning et al. 2013). Correspondingly, the carbon dissolved in a silicate melt coexisting with such a fluid is predominately in the form of either molecular CO_2 or the carbonate group (CO_3^{2-}), depending on temperature, pressure, and melt composition. However, under more reduced conditions such as in the Archean or at greater depths of the modern Earth, CH_4 together with some CO may prevail in C-O-H fluids (Ballhaus 1995; Kump and Barley 2007; Manning et al. 2013), and they dissolve into silicate melts differently. The solubility of carbon species (CO_2, CO, or CH_4) in a variety of silicate melts under a broad range of pressure and temperature conditions

1529-6466/13/0075-0009$00.00 DOI: 10.2138/rmg.2013.75.9

is crucial for understanding the degassing of Earth and other terrestrial planets, the formation of the atmosphere, as well as the petrogenesis of various igneous rocks.

In an earlier volume of the RiMG series published nearly two decades ago, Blank and Brooker (1994) and Holloway and Blank (1994) presented two excellent reviews on the solubility of CO_2 in silicate melts. Lately, Moore (2008) discussed some experimental and modeling aspects related to this topic. Since 1994, extensive new experimental data have been reported (e.g., Dixon et al. 1995; Brooker et al. 1999, 2001a,b; Botcharnikov et al. 2005, 2006; Lesne et al. 2011). Molecular dynamics simulations have recently been applied to the investigation of CO_2 solubility (Guillot and Sator 2011), which are particularly needed for pressures beyond 3 GPa. There have also been some other studies focusing on reduced conditions (e.g., Mysen et al. 2009; Morizet et al. 2010). Furthermore, considerable efforts have been made on the development of general CO_2 solubility models (e.g., Papale 1997, 1999; Papale et al. 2006). All post-1994 studies devoted to carbon solubility in silicate melts are listed in Table 1. Data from these studies are summarized in Online Supplementary Table 1.

Below, we will first discuss the work on CO_2 solubility in nominally anhydrous melts (the systems with CO_2 being the only volatile component), which is followed by a review of the studies on CO_2 solubility in hydrous melts (the systems with binary volatiles CO_2-H_2O), and followed by a summary on the solubility of C-O-H fluids under reduced conditions (the systems with ternary volatiles).

CO_2 solubility in nominally anhydrous melts

Experimental method. Solubility experiments are performed by saturating some melt with CO_2 at high pressure (P) and temperature (T) and then quenching the melt to a glass. The CO_2 content of the quenched glass is then measured by FTIR (Fourier transform infrared spectroscopy), SIMS (secondary ion mass spectrometry), or some other method and is assumed to represent the CO_2 solubility in the melt at given P and T. This method obviously can only be used for systems where melts can be quenched into homogeneous glasses, without quench crystallization and without bubble nucleation during quench. For this reason, CO_2 solubility data for non-quenchable utramafic melts do not exist and direct solubility measurements at deep mantle pressures > 10 GPa, where quenching melts to glasses becomes very difficult, are not available either. At pressures below 1 GPa, the liquidus temperatures of many water-free silicate melts are so high that measuring CO_2 solubility requires experiments in internally-heated gas pressure vessels equipped with a rapid-quench device.

The starting materials in CO_2 solubility experiments are either chips/powders of nominally anhydrous glass + silver oxalate or a mixture of oxides and carbonates, enclosed in noble metal capsules such as platinum or $Au_{80}Pd_{20}$. Silver oxalate $Ag_2C_2O_4$ decomposes upon heating to metallic silver and pure CO_2. It is the most commonly used source of CO_2 in high-pressure experiments and has largely replaced various organic compounds, such as oxalic acid, that were used in early studies. In addition, direct loading of gaseous CO_2 into the capsule has also been practiced (Botcharnikov et al. 2006, 2007). At superliquidus temperature (or a lower temperature at which the melt is metastable) and high pressure (see Moore 2008 for a discussion of various pressure vessels), it is expected that a silicate melt reaches equilibrium with a pure CO_2 fluid within a time frame of minutes to days. However, hydrogen can diffuse into the system through capsules, as evidenced by dissolved H_2O in quenched melts. If special care is taken in the experimental procedures, the dissolved H_2O can be controlled to below 4000 ppm or even 1000 ppm (Brooker et al. 1999). H_2O contents at such level are believed to have only a minor effect on the dissolution behavior of CO_2 (Stolper et al. 1987). In some circumstances, carbon (e.g., arising from a graphite heater in a piston-cylinder apparatus) may also gain access to the system, but this phenomenon can be avoided through the improvement of experimental design (Brooker et al. 1999). Hydrogen diffusing into the sample capsule may

not only introduce an additional, unwanted component, but it may also reduce CO_2 to other carbon species. Reduction may also be enhanced, perhaps through catalytic effects, by the capsule material, such as pure Pt. In order to retain carbon in the +4 oxidation state in such experiments, the oxygen fugacity therefore has to be kept high and diffusion of hydrogen into the capsule has to be suppressed as far as possible. In studies of Fe-bearing melts, the problem of iron loss to Pt can be alleviated by pre-saturating Pt capsules with Fe. Under high temperature and pressure, small amounts of melt components, such as alkali, may dissolve into the fluid phase. Despite all these experimental complexities, it is possible to produce a silicate melt of designated composition coexisting with a fluid with CO_2 mole fraction $X_{CO_2} > 90\%$, which can be treated approximately as a system with a single volatile component CO_2.

Analytical techniques. The CO_2 concentration in the glass quenched from a CO_2-saturated run gives the CO_2 solubility of a melt at a specific pressure and temperature, if the concentration remained unchanged during quenching. Under equivalent conditions, CO_2 solubility is one to two orders of magnitude lower than the solubility of H_2O. The low solubility of CO_2 and the limitation of then available analytical techniques (e.g., weight loss) caused early experimental studies to center on GPa level pressures. β-track autoradiography was once used frequently in carbon analysis (e.g., Mysen et al. 1975, 1976), but later it was found to yield inaccurate carbon concentration (Tingle and Aines 1988; Blank and Brooker 1994). FTIR has become by far the most frequently adopted analytical technique (Table 1) because it non-destructively probes both CO_2 and H_2O, measures concentrations down to ppm level with high accuracy, and delivers information about carbon speciation. The molar absorptivities of FTIR bands (2350 cm^{-1} for molecular CO_2 and the doublets within 1350-1650 cm^{-1} for CO_3^{2-}) for each specific melt composition need to be pre-calibrated by absolute methods (such as manometry or bulk carbon analyzers). Different authors may report CO_2 solubility based on different molar absorptivities, which is a major source of inconsistency between different data sets. Combined with stepped heating, it is plausible to separate adsorbed carbon, CO_2 from vesicles in the glass, and the actual dissolved carbon (e.g., Jendrzejewski et al. 1997). In addition to FTIR and the bulk analytical methods, SIMS and NMR (nuclear magnetic resonance) have also been occasionally used for carbon analysis (Pan et al. 1991; Thibault and Holloway 1994; Brooker et al. 1999; Behrens et al. 2004a).

Pressure effect. CO_2 solubility increases with increasing CO_2 fugacity and therefore with increasing pressure. Figure 1a shows that to the first order approximation, CO_2 solubility in rhyolite melt (at 1123-1323 K) and basalt melt (at 1473-1573 K) is proportional to pressure at $P < 0.7$ GPa with a common slope of about 0.57 ppm CO_2/bar (despite the fact that CO_2 speciation in quenched rhyolite and basalt glass is quite different). Therefore, approximately

$$C \propto P \tag{1}$$

where C is CO_2 solubility in ppm or wt% and P is pressure. The approximate proportionality between C and P may apply to pressures as high as 4.0 GPa, although the slope varies for different melts (Fig. 1b).

Phenomenologically, the proportionality between CO_2 solubility and pressure, which has been used for empirical fitting of CO_2 solubility (e.g., Liu et al. 2005), resembles Henry's law. But from a thermodynamic perspective, CO_2 must have the same chemical potential in the fluid phase and in the melt phase. The CO_2 chemical potential in the fluid is directly related to the fugacity f_{CO_2} (instead of pressure), and that in the melt is directly related to the activity (instead of mole fraction) of CO_2. There are many equations of state for pure CO_2 fluid available as summarized in Gottschalk (2007). For consistency we have adopted the EoS from Duan et al. (1992) to calculate f_{CO_2}, which is not much different (within 10%) from the reported fugacities in the original papers based on the EoS from Kerrick and Jacobs (1981) or earlier work. When CO_2 solubility is plotted against f_{CO_2}, their correlation deviates significantly from

Table 1. Studies on carbon solubility in silicate melts (since 1994).

Year	Authors	Melt	Fluid	*T* (°C)	*P* (bar)	Analytical Method
Data						
1994	Holloway & Blank	Basanite	CO_2	1200-1400	1000-20000	Bulk analyzer + SIMS
1995	Dixon et al.	Basalt	CO_2-H_2O	1200	310-980	FTIR
1997	Jakobsson	Andesite	CO_2-H_2O	1400	10000	FTIR + Bulk analyzer
1997	Jendrzejewski et al.	Basalt	CO_2	1200-1300	250-1950	Manometry + FTIR
1999	Brooker et al.	SNA	CO_2	1450-1700	10000-35000	Bulk analyzer + FTIR +NMR
2000	Paonita et al.	Rhyolite, Basalt	CO_2-H_2O-He	1130-1160	1120-2150	Estimated from Papale (1999) model
2001a,b	Brooker et al.	SNAC, MSNAC, Andesite, Phonolite, Nephelinite, Melilitite	CO_2	1175-1600	2000-27000	Bulk analyzer + FTIR
2001	Tamic et al.	Rhyolite	CO_2-H_2O	800-1100	2000-5000	FTIR
2002	King & Holloway	Andesite	CO_2-H_2O	1300	10000	FTIR
2002	Morizet et al.	Haplophonolite	CO_2	1300-1550	10000-25000	Bulk analyzer + FTIR
2004a	Behrens et al.	Dacite	CO_2-H_2O	1250	1000-5000	SIMS + FTIR
2004	Kadik et al.	Basalt	C-O-H	1520-1600	37000	MS
2005	Botcharnikov et al.	Basalt, Alkali Basalt	CO_2-H_2O	1150-1200	2000-5000	FTIR
2006	Botcharnikov et al.	Andesite	CO_2-H_2O	1100-1300	2000-5000	FTIR
2007	Botcharnikov et al.	Andesite	CO_2-H_2O-Cl	1200	2000	FTIR
2009	Behrens et al.	Phonotephrite	CO_2-H_2O	1200-1250	2000-5000	FTIR
2009	Mysen et al.	SN	C-O-H	1400	10000-25000	Bulk analyzer
2010	Morizet et al.	Haplobasalt	C-O-H	1250	2000-3000	FTIR
2010	Shishkina et al.	Basalt	CO_2-H_2O	1250	500-5000	FTIR
2011	Lesne et al.	Alkali Basalt	CO_2-H_2O	1200	269-2059	FTIR
2011	Vetere et al.	Trachyandesite	CO_2-H_2O	1250	500-4000	FTIR + Bulk analyzer
2011	Webster et al.	Rhyolite	CO_2-H_2O-S	897-1100	1990-2040	FTIR
2011	Stanley et al.	Basalt	CO_2	1400-1625	10000-25000	FTIR
2011	Guillot & Sator	Rhyolite, Basalt, Kimberlite	CO_2	1200-2000	1000-150000	Molecular dynamics
2012	Iacono-Marziano et al.	Alkali basalt, Lamproite,-kamafugite	CO_2-H_2O	1200	485–4185	FTIR
Model						
1997	Dixon	Basalt, Basanite, Leucitite, Melilitite	CO_2	1200-1400	0-20000	
1997	Papale	Various	CO_2	900-1600	0-30000	
1999	Papale	Various	CO_2-H_2O	700-1600	0-5000	
2002	Newman & Lowenstern	Rhyolite, Basalt	CO_2-H_2O	700-1500	0-5000	
2005	Liu et al.	Rhyolite	CO_2-H_2O	700-1200	0-5000	
2006	Papale et al.	Various	CO_2-H_2O	700-1600	0-10000	

For studies before 1994, see Table A1 and Table A2 in Blank and Brooker (1994). SNA = SiO_2-Na_2O-Al_2O_3 melts; SNAC = SiO_2-Na_2O-Al_2O_3-CaO melts; MSNAC = MgO-SiO_2-Na_2O-Al_2O_3-CaO melts.

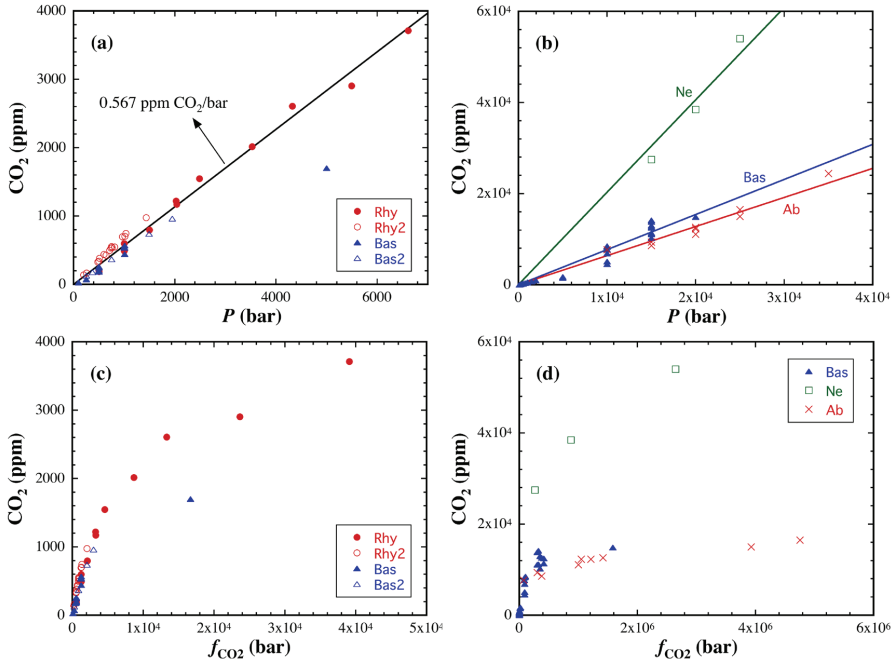

Figure 1. CO_2 solubility in anhydrous silicate melts (dissolved H_2O < 5000 ppm) versus pressure (in a,b) or CO_2 fugacity (in c,d). Data sources: Rhy = rhyolite melt at 1323 K (Fogel and Rutherford 1990); Rhy2 = rhyolite melt at 1123 K (Blank 1993); Bas = basalt melt at 1473 K (Stolper and Holloway 1988; Mattey 1991; Pan et al. 1991; Pawley et al. 1992); Bas2 = basalt melt at 1473-1573 K (Jendrzejewski et al. 1997); Ne = nepheline melt at 1973 K (Brooker et al. 1999); Ab = albite melt at 1723-1898 K (Stolper et al. 1987; Brooker et al. 1999). CO_2 fugacities are calculated from the equation of state for pure CO_2 fluid (Duan et al. 1992).

a proportional relationship at f_{CO_2} > 0.4 GPa (Fig. 1c,d). This nonlinearity can be attributed to the pressure dependence of CO_2 activity in the melt, which appears to compensate the non-ideal behavior of a real CO_2 fluid and cause the apparent proportionality between solubility and pressure.

Temperature effect. The influence of temperature on CO_2 solubility is less well constrained than the pressure influence. Blank and Brooker (1994) showed that after excluding the controversial data obtained using β-track autoradiography, CO_2 solubility decreases with increasing temperature, e.g., for rhyolite melt and albite melt (Fig. 2). Nevertheless, CO_2 solubility appears to be insensitive to temperature in basalt melt, and it even increases with increasing temperature in nepheline melt (Fig. 2). Furthermore, the direction of temperature effect may be reversed upon pressure change (Botcharnikov et al. 2005).

Composition effect. Compared to pressure and temperature effects, the dependence of CO_2 solubility on melt composition is more complex and more difficult to constrain. At ~1500 K and 0.2 GPa, CO_2 solubility increases weakly from rhyolite melt to dacite melt to andesite melt, but basalt melt and rhyolite melt have the lowest solubility (~1000 ppm) in the calc-alkaline series (Fig. 3a). On the other hand, CO_2 solubility increases nearly three-fold from basalt melt to alkali basalt melt to phonotephrite melt, all three of which have similar silica content. Therefore, CO_2 solubility appears to increase with increasing melt alkalinity, which is evidently demonstrated by a good correlation between solubility and total alkali content

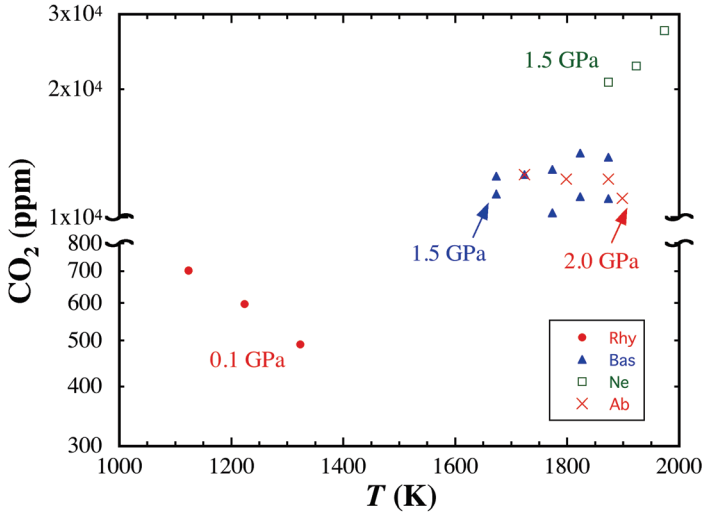

Figure 2. Temperature dependence of CO_2 solubility (in logarithmic scale) in anhydrous silicate melts (dissolved H_2O < 5000 ppm). Data sources: Rhy = rhyolite melt at 0.1 GPa (Fogel and Rutherford 1990; Blank 1993); Bas = basalt melt at 1.5 GPa (Pan et al. 1991); Ne = nepheline melt at 1.5 GPa (Brooker et al. 1999); Ab = albite melt at 2.0 GPa (Stolper et al. 1987; Brooker et al. 1999).

(Fig. 3b). The variation of CO_2 solubility with melt composition can be much more dramatic than illustrated in Figure 3. For example, Brooker et al. (2001a) showed that CO_2 solubility in a synthetic SNAC melt (35 wt% SiO_2, 10.5 wt% Al_2O_3, 49 wt% CaO, 5.5 wt% Na_2O) at 1500 K and 0.2 GPa can be as high as 8 wt%, which is about 80 times the solubility in basalt melt under equivalent conditions.

Molecular dynamics calculations. Most experimental solubility data fall within the pressure range of 0.01-3.0 GPa, with the only two exceptions being that Mysen et al. (1976) reported one datum (7.7 wt% CO_2) at 1898 K and 4.0 GPa in a melilitite melt and Brooker et al. (1999) reported one datum (2.44 wt% CO_2) at 1723 K and 3.5 GPa in albite melt. In principle solubility measurements could be extended to higher pressures by switching from a piston-cylinder apparatus to a multivanvil press, but there are numerous practical challenges. Complementarily, the solubility behavior at pressures > 3.0 GPa can now be investigated by molecular dynamics simulations.

Guillot and Sator (2011) performed the first molecular dynamics study on CO_2 solubility in silicate melts. A supercritical CO_2 fluid was numerically equilibrated with three natural melts at 1473-2273 K and 0.1-15 GPa. They found that CO_2 solubility increases more rapidly with the rise of pressure than predicted by the proportionality relationship, and that solubility decreases with increasing temperature (Fig. 4). The compositional dependence is weak among rhyolite melt, basalt melt and kimberlite melt at pressures below 8 GPa. They showed that their simulation results at low pressure are broadly consistent with experimental data.

Solubility model. Efforts were initially made (e.g., Stolper et al. 1987; Fogel and Rutherford 1990) to construct CO_2 solubility models for specific melt compositions, i.e., only the pressure (or fugacity) and temperature dependences were incorporated in the models. If CO_2 is treated as a simple component (i.e., CO_2 speciation in the melt phase is not accounted for), we consider the heterogeneous reaction

$$CO_2\ (fluid) = CO_2\ (melt) \qquad (2)$$

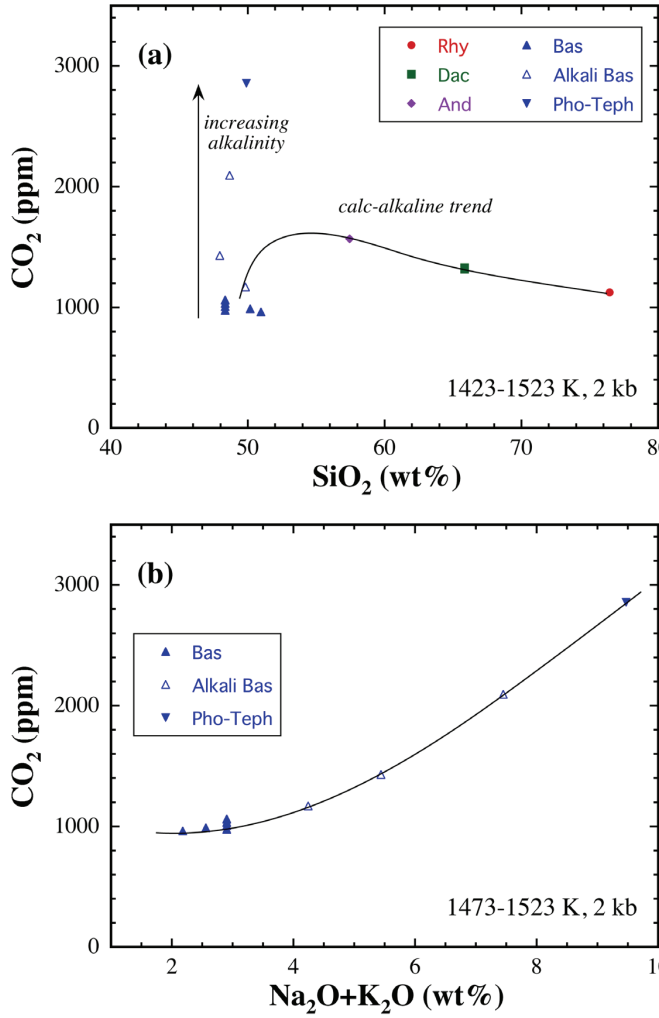

Figure 3. CO_2 solubility at 1423-1523 K and 0.2 GPa versus melt composition in anhydrous melts (the mole fraction of H_2O in the coexisting fluid phase is less than 0.1). Data sources: Rhy = rhyolite melt (Fogel and Rutherford 1990); Dac = dacite melt (Behrens et al. 2004a); And = andesite melt (Botcharnikov et al. 2006); Bas = basalt melt (Jendrzejewski et al. 1997; Botcharnikov et al. 2005; Shishkina et al. 2010); Alkali Bas = alkali basalt melt (Lesne et al. 2011); Pho-Teph = phonotephrite melt (Behrens et al. 2009). The curves are drawn to guide the eye.

The equilibrium constant K of the above reaction can be defined as

$$K = \frac{X_{CO_2}}{f_{CO_2}} \tag{3}$$

where f_{CO_2} is the CO_2 fugacity in the fluid phase and X_{CO_2} is the mole fraction of CO_2 in the melt phase. Note that unlike the unambiguous definition of CO_2 content of the melt in ppm or wt%, there are multiple ways defining the mole fraction of CO_2. If we limit our scope for treating a specific melt, the following definition is recommended,

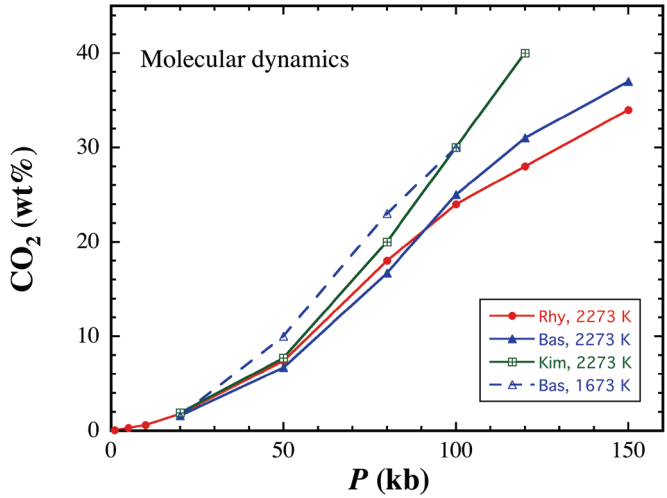

Figure 4. CO_2 solubility in anhydrous melts at 1673-2273 K based on molecular dynamics simulations. Rhy = rhyolite melt; Bas = basalt melt; Kim = kimberlite. Modified after Guillot and Sator (2011).

$$X_{CO_2} = \frac{\left(\frac{C}{44.01}\right)}{\left(\frac{C}{44.01} + \frac{(100-C)}{M}\right)} \tag{4}$$

where C is the CO_2 content of the melt in wt%, and 44.01 and M are the molecular weight of CO_2 and the formula weight of the volatile-excluded melt on a single oxygen basis (e.g., M = 32.78 g/mol for albite melt). Basically X_{CO_2} is proportional to C under realistic situations.

The equilibrium constant K varies with both pressure and temperature,

$$\left(\frac{\partial \ln K}{\partial P}\right)_{T,X} = -\frac{V}{RT} \tag{5a}$$

$$\left(\frac{\partial \ln K}{\partial T}\right)_{P,X} = \frac{\Delta H}{RT^2} \tag{5b}$$

where V is the partial molar volume of CO_2 in the melt, R is the gas constant, and ΔH is the molar dissolution enthalpy of CO_2 (ΔH is negative as the dissolution process is exothermic). If one sets the value of the equilibrium constant to be K_0 for a reference state (P_0, T_0), by combining Equation (3) and Equations (5a,b) we obtain

$$X_{CO_2} = f_{CO_2} K_0 \exp\left(\int_{P_0}^{P} -\frac{V}{RT}\mathrm{d}P + \int_{T_0}^{T} \frac{\Delta H}{RT^2}\mathrm{d}T\right) \tag{6}$$

With a further assumption that the pressure and temperature dependences of V and ΔH can be neglected, Equation (6) is simplified to the following form:

$$X_{CO_2} = f_{CO_2} K_0 \exp\left[\frac{V(P_0 - P)}{RT} + \frac{\Delta H}{R}\left(\frac{1}{T_0} - \frac{1}{T}\right)\right] \tag{7}$$

The above model correctly predicts a progressively gentler slope towards high P in solubility vs. fugacity plots (compare Fig. 1c,d) as well as a negative temperature dependence of CO_2 solubility. After designating a reference state (such as 1500 K and 1 atm) and selecting a valid equation of state of CO_2 fluid to calculate f_{CO_2}, one can fit experimental data $X(P, T)$ to Equation (7) and extract the three free parameters of K_0, V and ΔH (e.g., Fogel and Rutherford 1990).

Based on literature solubility data for melt compositions of basalt, basanite, leucitite and melilitite, Dixon (1997) presented a simple solubility model in which CO_2 solubility at 1473 K and 0.1 GPa is linearly correlated with the mole fractions of various cations. A more ambitious attempt was carried out by Papale (1997)—he compiled a large data set (263 data points) for various melt compositions and proposed a general CO_2 solubility model. The melt phase was regarded as a mixture of 11 oxide components SiO_2-TiO_2-Al_2O_3-Fe_2O_3-FeO-MnO-MgO-CaO-Na_2O-K_2O-CO_2 (hence the definition of CO_2 mole fraction was different from that in Eqn. 4). Papale (1997) presented a strict thermodynamic model based on the equivalence of CO_2 fugacity in the coexisting melt and fluid phases. However, he assumed that the partial molar volume of CO_2 in the melt coincides with that of pure CO_2 fluid, which was problematic and was discarded in their later models (Papale 1999; Papale et al. 2006). Compared to Equation (6), instead of extracting V and ΔH from fitting experimental data, the treatment in Papale (1997) is equivalent to assigning the volume of pure CO_2 fluid for V and assigning the enthalpy difference $H(P, T) - H(P_0, T)$ of pure CO_2 fluid for ΔH (at least mathematically). Also, K_0 in Equation (6) was replaced by a term related to the activity coefficient of CO_2 (γ) in the melt, which was again related to the excess Gibbs free energy of the melt (G^E). G^E was attributed to the interaction between oxide components according to the regular solution theory (here the compositional dependence weighs in). The interaction energy terms involving CO_2 were assumed to be pressure-dependent and were constrained by the experimental data.

The model of Papale (1997) reproduced 198 out of 263 solubility data to within 30%. But this model relied heavily on those early data involving β-track measurements. The large number of fitting parameters (22 in total not counting the interaction parameters between non-volatile components and not counting the designated reference pressure) compared to the limited number of melt compositions is also a cause for concern. Furthermore, the invariably positive temperature dependence (due to the replacement of dissolution enthalpy with $H(P, T) - H(P_0, T)$ of pure CO_2 fluid) is inconsistent with experimental observation. Special care should be taken when applying the Papale (1997) solubility model to pressures > 0.5 GPa and melts that are not covered by the data set used for modeling.

CO_2 solubility in hydrous melts

H_2O and CO_2 are considered to be the two most important volatile components in natural silicate melts. Numerous experiments have been performed to equilibrate a melt with a binary CO_2-H_2O fluid (Table 1), in which H_2O is loaded in the form of water or oxalic acid ($H_2C_2O_4$ or $H_2C_2O_4{\cdot}2H_2O$) (e.g., Dixon et al. 1995; Tamic et al. 2001). Even in some experiments where H_2O was not deliberately added to the system, careful examination of the quenched products indicated the presence of H_2O in both the melt phase and the fluid phase (e.g., Lesne et al. 2011).

Fluid composition analysis. The obtained CO_2 solubility in melt is meaningful only if the composition of the coexisting fluid can be characterized. One method is to separate the CO_2 from the H_2O of the fluid phase according to their different boiling point and then measure the amount of each component with gravimetry or manometry (e.g., Dixon et al. 1995; Jakobsson 1997; Shishkina et al. 2010). Another way of determining fluid composition is based on mass balance considerations together with the measurements of volatiles in the starting material and in the quenched melt (e.g., King and Holloway 2002).

CO_2-H_2O solubility data. Studies on CO_2-H_2O solubility often involve a series of experiments performed at the same pressure, temperature, and melt composition (on volatile-free basis) but with varying CO_2/H_2O ratios. The early experiments at pressures at GPa level (e.g., Mysen 1976) observed an initial increase in CO_2 solubility with the addition of H_2O and explained this with the depolymerization effect on the melt by H_2O. However, the measurements were made by β-track autoradiography, and the composition of the quenched fluid was unknown. By contrast, Blank (1993) and Dixon et al. (1995) showed for rhyolite melt and basalt melt at < 0.1 GPa that H_2O only causes a dilution effect lowering CO_2 fugacity and hence reducing CO_2 solubility in the melt. At a given temperature and pressure, CO_2 solubility should be proportional to f_{CO_2} (Henrian behavior; Eqn. 3 with K being a constant) and should also be proportional to CO_2 fraction in the fluid phase (here denoted as Y_{CO_2}) because the CO_2 fugacity coefficient does not vary significantly with CO_2/H_2O at temperatures far above 1000 °C and pressures not higher than a few GPa.

Experimental results for a variety of silicate melts obtained at 0.2-1.0 GPa are summarized in Figure 5. The behavior of CO_2 solubility at these intermediate pressures appears to be in the middle of the behavior at higher pressures (Mysen 1976) and that at lower pressures (Blank 1993; Dixon et al. 1995). Only one study on andesite melt at 1.0 GPa (King and Holloway 2002) observed a positive correlation between the dissolved CO_2 and the dissolved H_2O (Fig. 5b), in agreement with Mysen (1976). All the other studies generally showed a negative correlation between CO_2 and H_2O within each individual data set, but CO_2 solubility flattens out when the concentration of dissolved H_2O becomes sufficiently low (Fig. 5a,b). At pressures of 0.5 GPa or higher, CO_2 solubility is nearly constant over a broad H_2O concentration range. Plots of CO_2 solubility versus CO_2 fraction in the fluid phase or CO_2 fugacity (Fig. 5c-f) demonstrate a nonlinear correlation (the deviation from linearity enlarges as pressure increases), which suggests an evident non-Henrian behavior. In addition, the data of rhyolite, dacite, andesite, and basalt suggest that the compositional effect becomes more pronounced at higher pressure (Fig. 5a,c,e). At 1.0 GPa, CO_2 solubility in icelandite (ferroandesite) melt is roughly three times larger than that in andesite melt (Fig. 5b-d).

There have also been a few studies with an extra volatile component such as He, Cl, or S in addition to CO_2 and H_2O (Paonita et al. 2000; Botcharnikov et al. 2007; Webster et al. 2011), but these studies typically emphasize the effect of CO_2 on the solubility of the extra volatile component rather than CO_2 solubility itself.

CO_2-H_2O solubility models. Based on several experimental studies and the assumption of Henrian behavior for CO_2-H_2O dissolution, Newman and Lowenstern (2002) developed a program VolatileCalc that can be used in Excel to calculate the solubility of CO_2-H_2O in rhyolite melt and basalt melt at 700-1500 °C and less than 0.5 GPa. However, the CO_2-H_2O solubility data in Tamic et al. (2001) showed marked deviation from the predictions by VolatileCalc. Liu et al. (2005) provided an easy-to-use empirical expression of CO_2 solubility in rhyolite melt as a function of the partial pressure of H_2O and that of CO_2, applicable to 700-1200 °C and 0.5 GPa. Figure 6 presents the calculation results for rhyolite melt at 1373 K according to the VolatileCalc program and the model of Liu et al. (2005). The feature of CO_2 solubility first increasing with H_2O concentration in Figure 6b may be an artifact due to some inconsistency between the CO_2 solubility data of Fogel and Rutherford (1990) and the CO_2-H_2O solubility data of Tamic et al. (2001), based on which the model of Liu et al. (2005) was constructed.

Papale (1999) extended his previous model on pure CO_2 or pure H_2O solubility (Papale 1997) to the solubility of two-component CO_2-H_2O fluids in 12-component (10 oxides + 2 volatiles) silicate melts. Papale et al. (2006) updated the model of Papale (1999) by adding a large amount of new CO_2-H_2O solubility data and discarding the pre-1980 CO_2 solubility data (mostly from β-track autoradiography). The highlight of Papale (1999) and Papale et al. (2006) was again the treatment of compositional dependences. Unlike Papale (1997), the

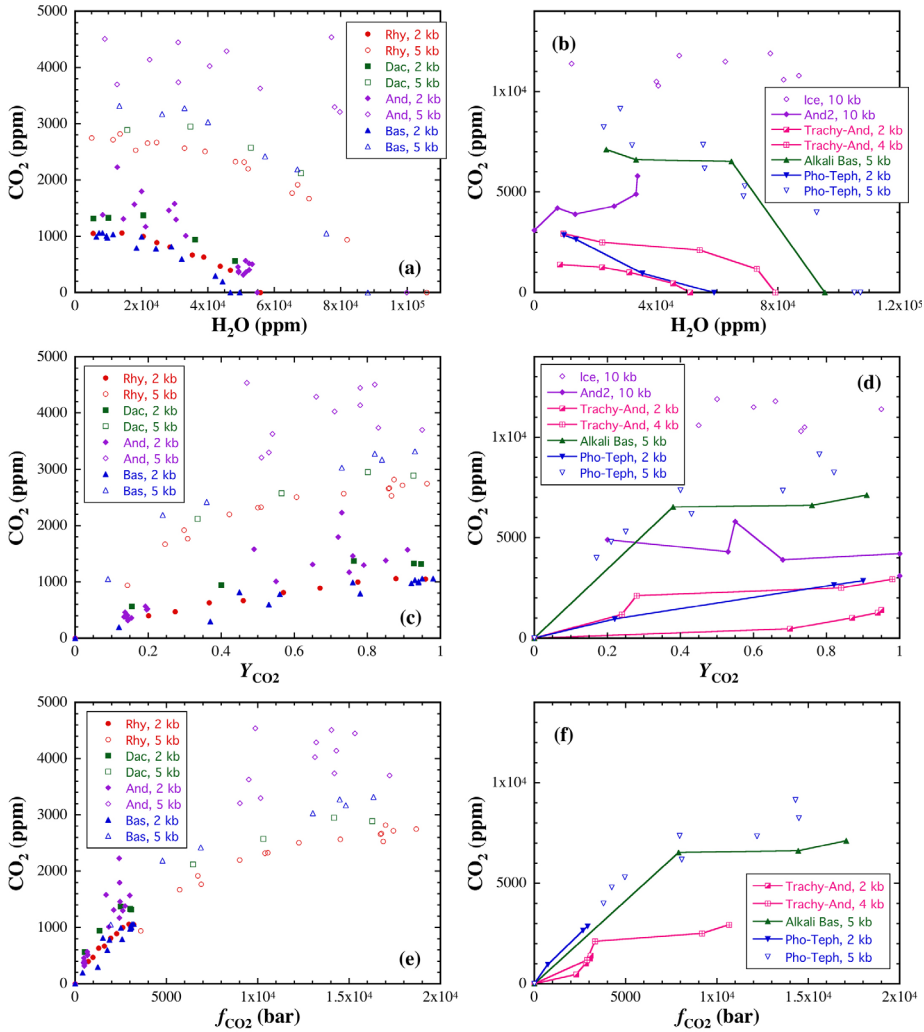

Figure 5. CO_2 solubility in hydrous silicate melts versus H_2O content (a,b), CO_2 fraction in the coexisting fluid (c,d), and CO_2 fugacity (e,f). Data sources: Rhy = rhyolite melt at 1373 K (Tamic et al. 2001); Dac = dacite melt at 1523 K (Behrens et al. 2004a); And = andesite melt at 1373-1573 K (Botcharnikov et al. 2006, 2007); Bas = basalt melt at 1473-1523 K (Botcharnikov et al. 2005; Shishkina et al. 2010); Ice = icelandite melt at 1673 K (Jakobsson 1997); And2 = andesite melt at 1573 K (King and Holloway 2002); Trachy-And = trachyandesite (shoshonite) melt at 1523 K (Vetere et al. 2011); Alkali Bas = alkali basalt melt at 1423 K (Botcharnikov et al. 2005); Pho-Teph = phonotephrite melt at 1473-1523 K (Behrens et al. 2009). CO_2 fugacities are derived from the equation of state for CO_2-H_2O fluids (Duan and Zhang 2006).

partial molar volume of CO_2 in the melt was assumed to be a 10-parameter (Papale 1999) and 3-parameter (Papale et al. 2006) function of pressure and temperature. Fitting of the experimental data indicated that the interaction between CO_2 and H_2O in the melt contributes negligibly to the excess Gibbs free energy of the melt. Papale et al. (2006) showed that their model reproduces most of the 173 CO_2 solubility data and 84 CO_2-H_2O solubility data (in terms of saturation pressure) within 25% relative.

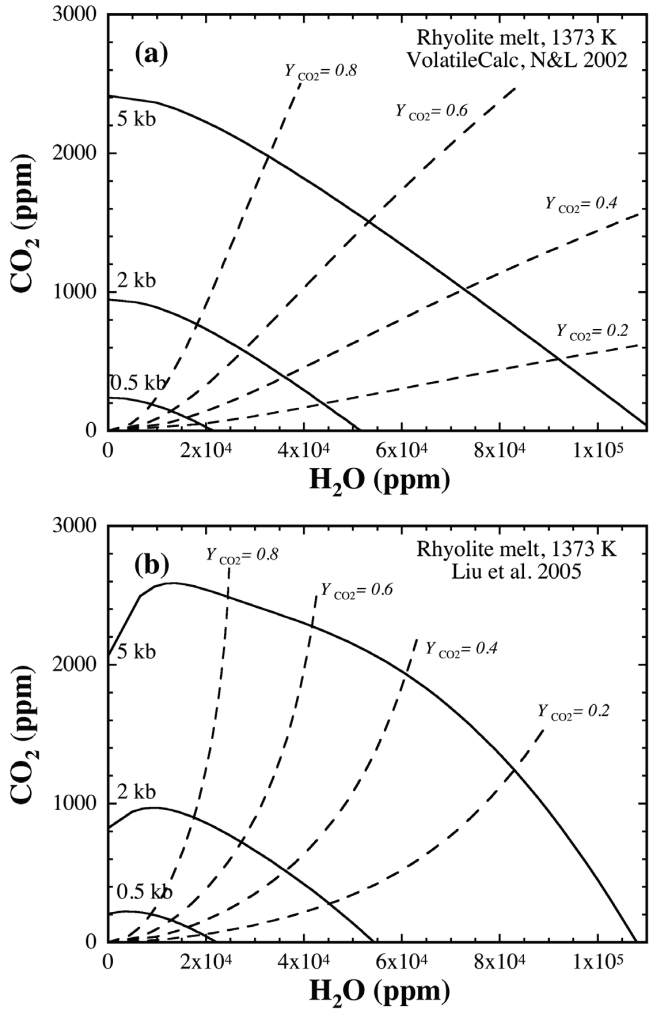

Figure 6. CO_2-H_2O solubility in rhyolite melt at 1373 K based on (a) the VolatileCalc program of Newman and Lowenstern (2002); and (b) the empirical model of Liu et al. (2005). The solid curves represent isobaric saturation, and the dashed curves represent fixed CO_2 mole fractions in the coexisting fluid phase.

The thermodynamic model of Papale et al. (2006) has indicated non-Henrian behavior of CO_2-H_2O solubility in rhyolite melt and basalt melt at high pressure (Fig. 7), in contrast with the Henrian behavior predicted by VolatileCalc (Fig. 6a). Based on Papale et al. (2006), for rhyolite melt at 0.5 GPa, CO_2 solubility first increases with dissolved H_2O in the melt; but for basalt melt at 0.5 GPa, CO_2 solubility decreases rapidly with the initial addition of H_2O. Later experimental data have demonstrated limited success of the Papale et al. (2006) model. Shishkina et al. (2010) showed that this model always underestimates volatile saturation pressure (in other words, the model overestimates CO_2-H_2O solubility) for basalt melt, opposite to the estimation by the VolatileCalc program (Fig. 8a). Furthermore, the non-ideality of CO_2-H_2O solubility in basalt melt is smaller than predicted by the Papale et al. (2006) model (Shishkina et al. 2010). There is also large disparity between the data for alkali basalt melt

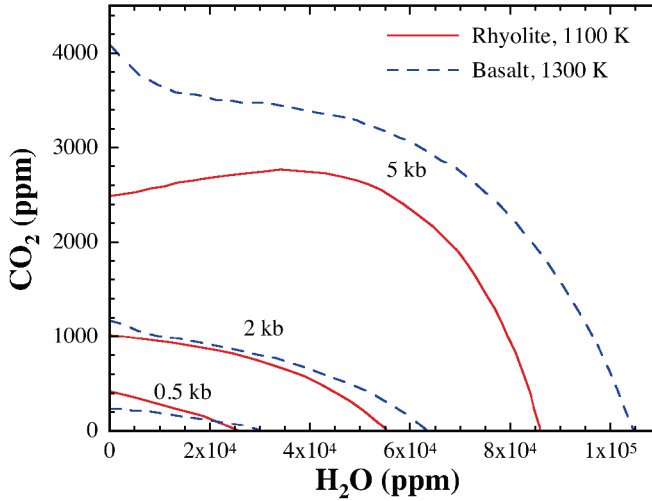

Figure 7. CO_2-H_2O solubility in rhyolite melt at 1100 K (solid curves) and basalt melt at 1300 K (dashed curves) based on the thermodynamic model of Papale et al. (2006).

(Lesne et al. 2011) and the model. Vetere et al. (2011) showed that the deviation between their data for trachyandesite melt at 0.05 GPa and 0.2 GPa and the model of Papale et al. (2006) is significant, but the data at 0.4 GPa agree with the model (Fig. 8b). The Papale et al. (2006) model may therefore need recalibration by new experimental data.

Solubility of C-O-H fluids under reduced conditions

The Archean Earth or certain deep regions in Earth's mantle today may be reduced enough for CO or CH_4 to be significant components in C-O-H fluids (Ballhaus 1995; Kump and Barley 2007; Frost and McCammon 2008). These species are expected to have different dissolution behavior in silicate melts.

CO-CO₂ solubility. At constant temperature and pressure, the CO/CO_2 ratio of a C-O fluid increases with decreasing oxygen fugacity until graphite saturation is reached (Fig. 9a). Under graphite saturation,

$$C(s) + CO_2(f) = 2CO(f) \quad (8)$$

where "*s*" and "*f*" denote the solid graphite phase and the fluid phase, respectively. The proportions of the two species calculated from the equilibrium constant of the above reaction vary significantly with temperature and pressure (Fig. 9b), which can be checked with post-experiment analysis on the fluid phase or the fluid inclusions in quenched glass (Pawley et al. 1992).

Eggler et al. (1979) showed for several melts that CO-CO_2 solubility is comparable (lower at subliquidus temperatures but higher at superliquidus temperatures) with the solubility of pure CO_2, and argued that CO is also soluble in silicate melts. However, their data were acquired by the potentially unreliable β-track autoradiography. On the contrary to Eggler et al. (1979), Pawley et al. (1992) demonstrated that at < 0.15 GPa the dissolved carbon (in the form of CO_3^{2-}) in a basalt melt is proportional to CO_2 fugacity, and hence concluded that the role of CO is limited to diluting CO_2 (i.e., the solubility of CO in the melt is much smaller than that of CO_2).

Solubility of reduced C-O-H fluids. Holloway and Jakobsson (1986) and Jakobsson and Holloway (1986) investigated the solubility of C-O-H fluids in several silicate melts at 1.0-2.5

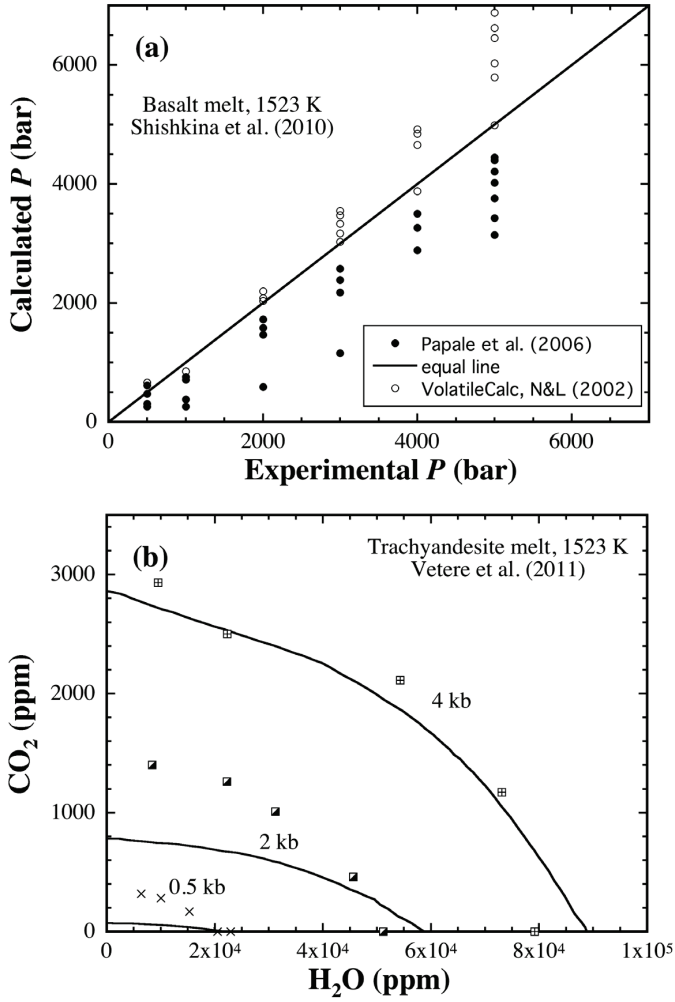

Figure 8. (a) CO_2-H_2O saturation pressure calculated from the Papale et al. (2006) model (solid circles) and the VolatileCalc program (open circles) of Newman and Lowenstern (2002) versus experimental pressure for basalt melt at 1523 K. After Shishkina et al. (2010). (b) Experimental CO_2-H_2O solubility in trachyandesite melt at 1523 K compared to the Papale et al. (2006) model (solid curves). After Vetere et al. (2011).

GPa under graphite saturation at the iron-wüstite (IW) buffer. For a given temperature and pressure, these two constraints (carbon activity is one and oxygen fugacity is at IW buffer) together with the mass balance constraint and the equilibrium constants of the following reactions,

$$CO + \frac{1}{2}O_2 = CO_2 \quad (9a)$$

$$H_2 + \frac{1}{2}O_2 = H_2O \quad (9b)$$

$$CO + 3H_2 = CH_4 + H_2O \quad (9c)$$

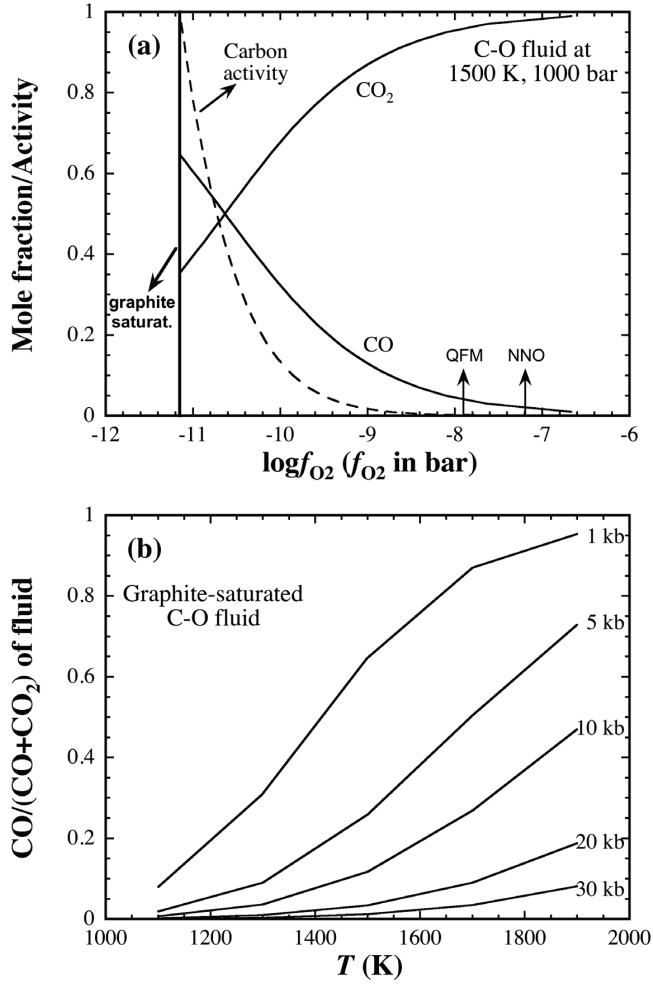

Figure 9. (a) The change of CO_2 and CO mole fractions (solid curves) and carbon activity (dashed curve) with oxygen fugacity for C-O fluid at 1500 K and 0.1 GPa. Oxygen buffers of NNO and QFM are indicated in short vertical arrows. CO_2 fraction approaches minimum at graphite saturation (carbon activity equals 1). (b) CO fraction of graphite-saturated fluid at various temperatures and pressures. Calculations are based on the standard thermodynamic data in the JANAF table (Chase 1998) and the fugacity coefficients using the GFluid program (Zhang and Duan 2010).

fix the composition of the fluid (the fractions of CH_4, CO, CO_2, H_2, O_2, and H_2O). Under the experimental conditions of Holloway and Jakobsson (1986) and Jakobsson and Holloway (1986), the dominating volatile species are CH_4 and H_2O, with minor amounts of H_2 and CO (Fig. 10). Jakobsson and Holloway (1986) suggested that CO is more soluble than CO_2 and CH_4 in silicate melts. However, their conclusion was purely based on quadrupole mass spectrometry. There was no FTIR or Raman evidence for the presence of molecular CO in the melt. Furthermore, high CO solubility appears to be inconsistent with low-pressure studies (Pawley et al. 1992; Morizet et al. 2010).

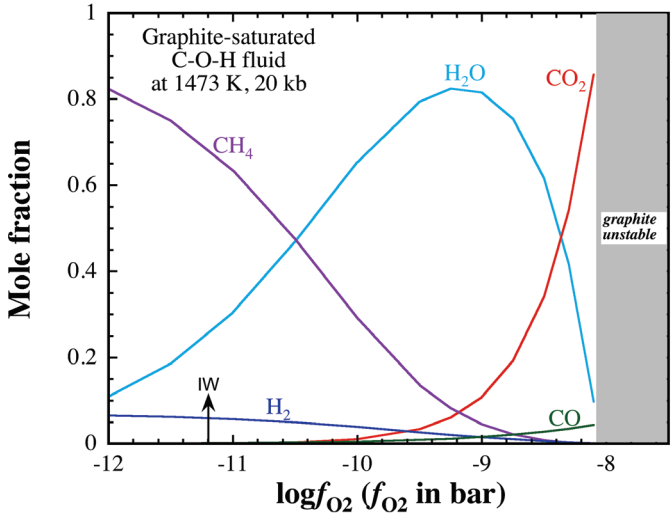

Figure 10. Mole fractions of various species in C-O-H fluid at 1473 K, 2.0 GPa and graphite saturation, calculated with the GFluid program (Zhang and Duan 2010). Oxygen buffer of iron-wüstite (IW) is indicated in short vertical arrow.

Kadik et al. (2004) also investigated the dissolution of C-O-H species in ferrobasalt melt at 3.7 GPa and 1800-1873 K under graphite saturation and IW buffer conditions. Their IW buffer fixed hydrogen fugacity instead of oxygen fugacity because it was placed outside the capsule, hence ΔIW with respect to oxygen was about −2.4. The system was so reduced that an iron metallic phase formed at equilibrium. Strictly speaking, their experiments were not really a solubility study under our definition as a fluid phase was absent. They concluded that the dissolved carbon (1600 ppm as C) should mostly be either atomic or amorphous based on the lack of observable bands in FTIR and Raman spectroscopy. Mysen et al. (2009) showed that CH_4 is quite soluble (2000-5000 ppm as CH_4) in Na_2O-SiO_2 melts at 10-2.5 GPa and 1673 K as molecular CH_4 or possibly species containing C≡C–H bonds. However, the composition of the coexisting fluid in their experiments was not examined, and may not be a binary oxygen-free CH_4+H_2 mixture as assumed. Under extremely reduced conditions (ΔIW ranging from −3.7 to −5.6 with respect to oxygen fugacity), Kadik et al. (2006, 2010, 2011) reported that the carbon dissolved in graphite-saturated iron-bearing melts at 1.5-4.0 GPa and 1673-1873 K was present as CH_4 species, based on Raman spectroscopy. Note that similar to Kadik et al. (2004), there was no free C-O-H fluid phase in coexistence with the melt.

Morizet et al. (2010) used Ar-H_2 gas as the pressure medium of internally-heated pressure vessels to produce intermediate reduced conditions (ΔQFM within ±2.6), under which CO_2, H_2O, and CO are the major species in the fluid phase. Based on a series of experiments at 1523 K and 0.2-0.3 GPa, they concluded that CH_4 and CO are essentially insoluble in haplobasalt melt.

CARBON SPECIATION IN SILICATE MELTS

Spectroscopic information on speciation

Infrared and Raman spectroscopy. Infrared and Raman spectroscopy are two types of vibrational spectroscopy, i.e., they probe the interaction of electromagnetic radiation with vibrations that occur in a molecule or in a condensed phase. The information obtained from

both types of spectroscopy can be complementary, as due to different selection rules, some vibrations may only be detected in the infrared spectrum, while others are only Raman active. The normal modes (independent vibrations) of molecular CO_2 are shown in Figure 11 and Table 2, and those of the carbonate ion (CO_3^{2-}) are shown in Figure 12 and and Table 3. For the linear CO_2 molecule containing 3 atoms, there are $3 \times 3 - 5 = 4$ independent vibrations. Both the symmetric bending vibration at 667 cm^{-1} and the antisymmetric stretching vibration at 2349 cm^{-1} are infrared active; however, in silicate glasses, there is strong absorption from the glass matrix in the frequency range of the bending vibration, so that normally it cannot be observed. The antisymmetric stretching vibration is prominent in the spectra of glasses containing molecular CO_2 (Fig. 13), as the corresponding extinction coefficients are high and the absorption from the glass matrix in this frequency region is negligible. The symmetric stretching vibration near 1337 cm^{-1} may be observed in Raman spectra of CO_2-bearing glasses. Fortuitously, this frequency is nearly twice the frequency of the symmetric bending vibration at 667 cm^{-1}. In this situation, Fermi resonance may occur, where the first overtone of the bending vibration gains intensity by interaction with the symmetric stretching vibration. Therefore, a pair of bands ("Fermi diade") may be observed in the Raman spectrum of CO_2 gas, while usually only one band near 1382 cm^{-1} is seen in the spectra of glasses containing molecular CO_2 (Fig. 14). This can be useful to distinguish CO_2 in gas bubbles from CO_2 dissolved in the glass (e.g., Brooker et al. 1999).

For the carbonate group, there are $3 \times 4 - 6 = 6$ independent vibrations. As with molecular CO_2, the bending vibrations are usually hidden by the absorbance of the glass matrix in the infrared spectrum. However, the ν_3 antisymmetric stretching vibration is very intense in the infrared spectrum and only slightly overlaps with background absorption from the glass matrix. As noted in Table 3, this vibration is twofold degenerate, i.e., there are two physically different vibrations (with atoms vibrating in different directions), which in the undistorted CO_3^{2-} group have the same frequency. This is obvious from Figure 12: Rotating the image showing the movement of atoms during the antisymmetric stretching vibration by 120° or 240° produces vibrations of the same type, but with individual atoms moving in different directions. A more thorough analysis shows that of these three vibrations, only two are independent, the third one can be produced as a combination of the other two vibrations. The degeneracy of these

Table 2. Internal vibrations of the CO_2 molecule

Mode	Selection rule	Frequency (cm^{-1})
ν_1 symmetric stretch	Raman	1337
ν_2 symmetric bend	IR	667
ν_3 asymmetric stretch	IR	2349

The ν_2 symmetric bending vibration is two-fold degenerate, i.e., there are two physically different vibrations, which in a free molecule have the same frequency for symmetry reasons.

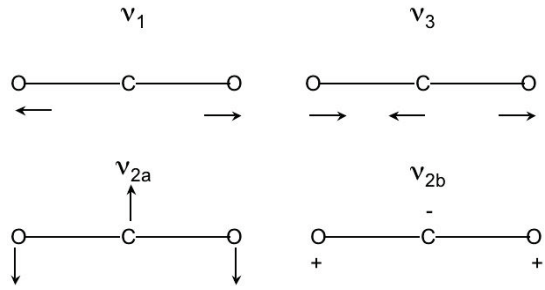

Figure 11. Normal modes of the CO_2 molecule

Table 3. Internal vibrations of the carbonate group

Mode	Symmetry	Selection rule	Frequency (cm^{-1})
ν_1 symmetric stretch	A_1'	Raman	1063
ν_2 out-of-plane bend	A_2'	IR	879
ν_3 asymmetric stretch	E′	IR + Raman	1415
ν_4 in-plane bend	E′	IR + Raman	680

The ν_3 and ν_4 vibrations are both two-fold degenerate, i.e., there are two physically different vibrations each, which in an undistorted carbonate group have the same frequency for symmetry reasons. Symmetry types are for trigonal D_{3h} symmetry.

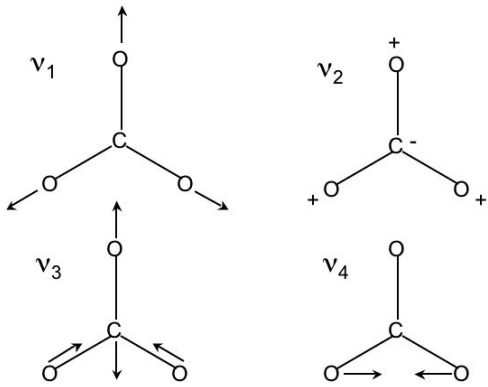

Figure 12. Normal modes of the carbonate group (CO_3^{2-}), for ideal trigonal D_{3h} geometry.

vibrations, however, will disappear if the environment of the carbonate group is asymmetric, e.g., if one of the oxygen atoms is more strongly bonded than the others. In such a situation, the two vibrations will have different frequencies and the asymmetric stretching vibration in the infrared spectrum will split into two components. This effect is observed in carbonate-bearing silicate glasses (Fig. 13) and the type of splitting observed contains valuable information about the environment of the carbonate group. Note that whatever the distortion in the environment of the carbonate group is, only one band (in a symmetric environment) or two bands (in a distorted environment) may be produced by one type of carbonate group. If there are more bands, there must be more structurally different carbonate groups. In theory, two infrared bands could also be produced by two structurally different carbonate groups, each residing in a symmetric environment. In such a situation, however, the Raman spectrum should also show two symmetric stretching bands at different frequencies and separate carbonate peaks should also be observed in the NMR spectrum. The most prominent band in the Raman spectrum of carbonate is the symmetric stretching vibration at 1063 cm^{-1}, which, however, often overlaps with the Si-O stretching vibrations of the glass matrix (Fig. 14).

Infrared spectroscopy measures absorption of infrared radiation, while Raman spectroscopy measured light scattering, often in the visible range. In general, infrared spectra can be more easily quantified than Raman spectra, since absorbance can routinely be measured with an accuracy of 1% relative or better. For this reason and because the infrared bands of the antisymmetric stretching vibrations of CO_2 and carbonate are well separated from the absorbance of the glass matrix, infrared spectroscopy has been used extensively to study the speciation of carbon in silicate glasses. Moreover, it has also been widely used as an analytical tool to derive CO_2 contents from the measured absorbance for CO_2 and carbonate using the Lambert Beer law $A = \varepsilon\, c\, d$, where A is linear or integral absorbance, ε is the molar extinction

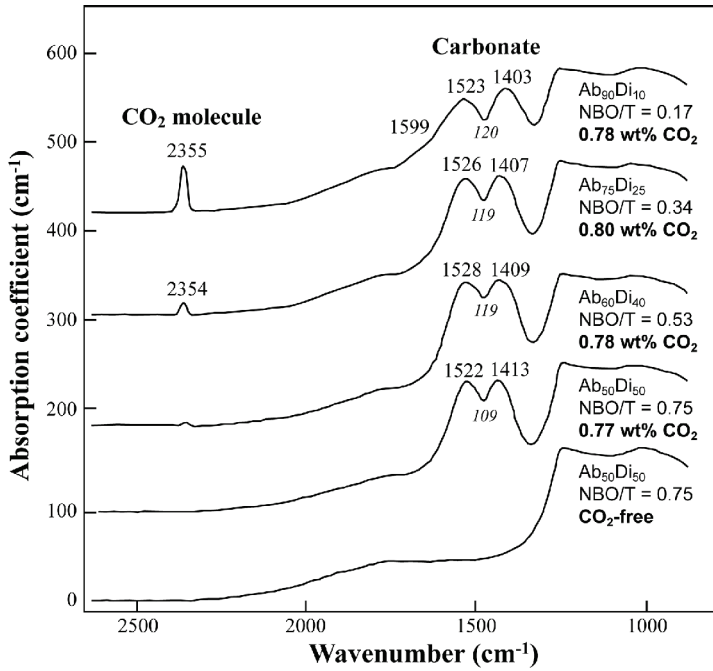

Figure 13. Infrared spectra of some CO_2-bearing glasses along the albite ($NaAlSi_3O_8$) - diopside ($CaMgSi_2O_6$) join. Bulk CO_2 content is about 0.8 wt%. While molecular CO_2 and carbonate coexist in the albite-rich compositions, the more diopside-rich compositions only contain carbonate. Note the splitting of the carbonate band into two components due to a low-symmetry environment. After Konschak (2008).

coefficient, c is concentration (in mol/l), and d is the sample thickness. Extinction coefficients of both molecular CO_2 and carbonate are matrix-dependent and need to be calibrated against some other analytical method that measures absolute carbon. Extinction coefficients for the antisymmetric stretching vibrations of molecular CO_2 and of carbonate are compiled in Table 4.

NMR spectroscopy. ^{13}C NMR (nuclear magnetic resonance) spectroscopy probes the chemical environment of a ^{13}C nucleus by measuring the energy required to change the orientation of this nucleus in a very strong external magnetic field (several Tesla). The local field seen by the nucleus will be shielded by the surrounding electron shell. Therefore, there is a chemical shift of the absorption frequency depending on the chemical environment of the nucleus; this shift is usually given as shift in ppm (i.e., 10^{-6}) relative to a standard (TMS, tetramethylsilane). In a solid material, such as a glass, dipolar interactions between neighboring nuclei will tend to broaden NMR peaks to such an extent that no structural information can be obtained. This effect can be suppressed by rapid (kHz) rotation of the sample at the magic angle (54°44′) relative to the magnetic field. This MAS (magic angle spinning) technique is therefore routinely used to acquire ^{13}C NMR spectra of carbon-bearing glasses (Fig. 15). Compared to infrared spectroscopy, ^{13}C NMR has been less frequently used to study carbon in glasses, however, it can yield useful complementary information. One particular advantage of ^{13}C NMR is that it is intrinsically quantitative; the areas of the NMR peaks are directly proportional to species abundance, or in other words, the intensity ratio of two peaks directly gives the abundance ratio of the corresponding species. Moreover, all carbon species in a sample will be detected, even if they do not possess any infrared active bands or bands that are only weak or overlap with other bands in the infrared spectrum.

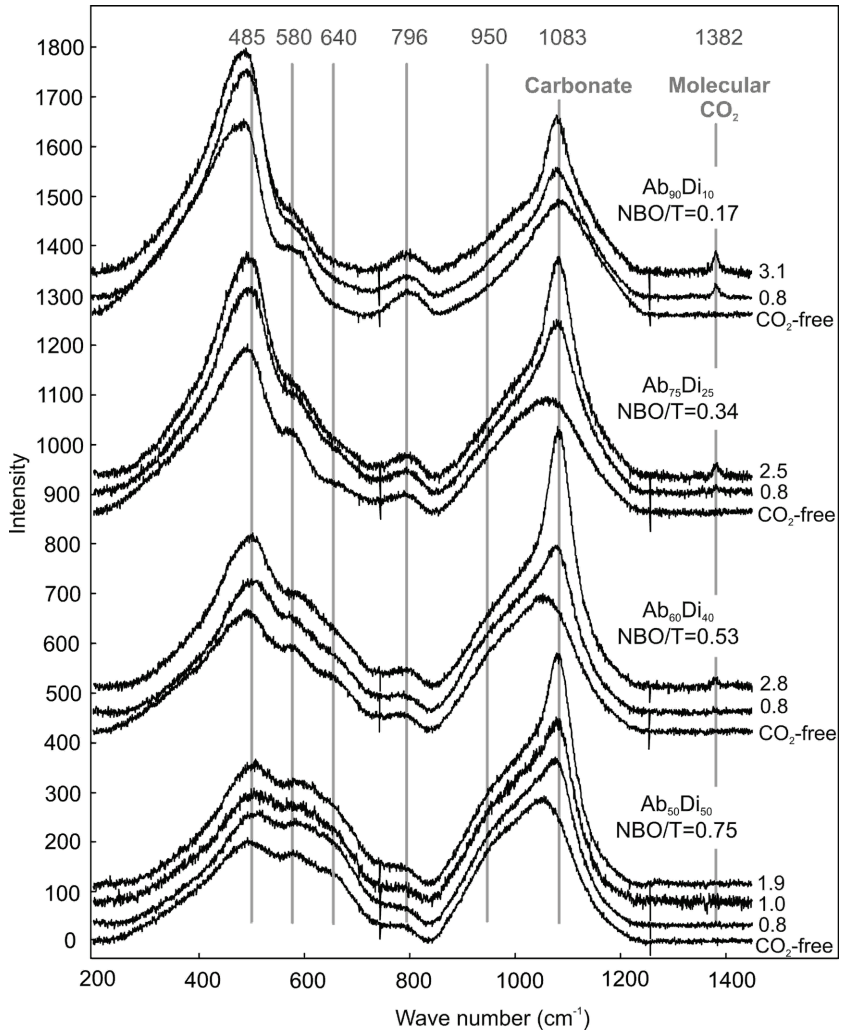

Figure 14. Raman spectra of some CO_2-bearing glasses along the albite ($NaAlSi_3O_8$) - diopside ($CaMgSi_2O_6$) join. For each glass composition, spectra with different bulk CO_2 content (in wt%) are shown. After Konschak (2008).

Carbon speciation in silicate glasses

Variation of carbonate and molecular CO_2 as function of glass composition. Wyllie and Tuttle (1959) noted that the differences in CO_2 solubility between felsic and mafic or ultramafic melts are likely due to the formation of carbonate in the latter compositions. Indeed, infrared and Raman spectroscopic studies of glasses later showed (e.g., Brey 1976; Fine and Stolper 1986; Stolper et al. 1987) that all CO_2 is dissolved as carbonate in basaltic glasses, while rhyolite, albite and other silica-rich glasses contain molecular CO_2 coexisting with at most minor amounts of carbonate. In andesite and phonolite glasses, molecular CO_2 and carbonate coexist (e.g., Brooker et al. 2001b). If melt compositions are expressed as NBO/T (i.e., non-bridging oxygen atoms per tetrahedron), increasing NBO/T or depolymerization of the melt

Table 4. Infrared extinction coefficients ε of CO_2 and carbonate group in silicate glasses

Composition	Reference	integral ε of CO_2 (L mol^{-1} cm^{-2})	linear ε of CO_2 (L mol^{-1} cm^{-1})	integral ε of CO_3^{2-} (L mol^{-1} cm^{-2})	linear ε of CO_3^{2-} (L mol^{-1} cm^{-1})	carbonate band (cm^{-1}) for linear ε
Albite – jadeite	Fine & Stolper (1985)	25 200 ± 1200	945 ± 45	24 100 ± 1900* 16 800 ± 1500 *	200 ± 15 235 ± 20	1610 1375
Albite	Nowak et al. (2003)	18 000 ± 1000		42 250 ± 2000		
Rhyolite	Behrens et al. (2004b)		1214 ± 78			
Dacite	Nowak et al. (2003)	16 000 ± 1000		40 100 ± 2000		
Dacite	Behrens et al. (2004a)		830		170	1530
Icelandite	Jakobsson (1997)			54450 27730* 27700*	 180 190	 1500 1420
Phonotephrite	Behrens et al. (2009)				308 ± 110	1430
Basanite	Dixon & Pan (1995)			60 000 ± 1700	283 ± 8	1525 and 1425
Ca-rich leucitite	Thibault & Holloway (1994)				340 ± 20	1515
Basalt**	Fine and Stolper (1986)			69500 ±3000	375 ± 20	1515 and 1435
Basalt	Shishkina et al. (2011)				317 ± 23	1430
Ferrobasalt	Stanley et al. (2011)			81500 ± 1500		
Shoshonite	Vetere et al. (2011)				356 ± 18	1430

Integral extinction coefficients are calibrated using the peak area, while linear extinction coefficients refer to peak height. For carbonate, there are usually two bands in the range of 1350 - 1650 cm^{-1}. The integral extinction coefficients refer to the integral under both bands, unless otherwise noted, while the linear extinction coefficients refer to the height of one band, which is specified in the last column of the table. All data for molecular CO_2 refer to the band near 2351 cm^{-1}. * these integral extinction coefficients refer to the individual carbonate bands specified in the last column. **this calibration includes basalt, diopside and a calcium aluminosilicate glass

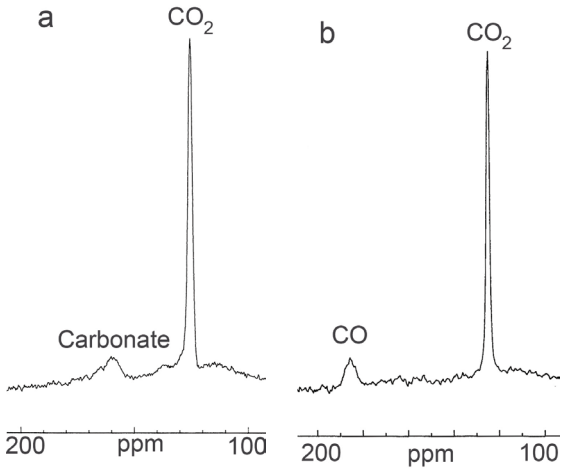

Figure 15. ^{13}C NMR spectra of CO_2-bearing silicate glasses. (a) CO_2 in hydrous albite glass. Note the asymmetry of the carbonate peak, suggesting the presence of more than one carbonate species. (b) CO_2 in rhyolite glass containing some CO and a trace of carbonate. Spectra courtesy of Simon Kohn.

favors the formation of carbonate in the glasses at the expense of molecular CO_2. This effect is illustrated in the infrared spectra of some glasses along the albite ($NaAlSi_3O_8$) - diopside ($CaMgSi_2O_6$) join in Figure 13. The corresponding Raman spectra are shown in Figure 14. Note that in the infrared spectrum, the degeneracy of the antisymmetric stretching vibration of carbonate is lifted, producing two bands separated by 109-120 cm^{-1}. On the other hand, there is one single symmetric stretching vibration of carbonate at 1083 cm^{-1} in the Raman spectrum (overlapping with the Si-O stretching vibrations), which confirms that these glasses contain one single type of carbonate group in some asymmetric environment. For the albite-rich compositions, both the Raman and infrared spectra show only one band for molecular CO_2, the antisymmetric stretching vibration in the infrared spectra at 2355 cm^{-1} and the symmetric stretching vibration at 1382 cm^{-1} in the Raman spectra. Data from ^{13}C NMR spectra (Fig. 15) are generally consistent with the speciation models derived from infrared spectra.

Given that the relative abundance of molecular CO_2 and carbonate appear to depend on the availability on non-bridging oxygen atoms in the glass, one may write equilibrium of the type:

$$CO_2 + O^{2-} = CO_3^{2-} \quad (10)$$

where "O^{2-}" stands for a non-bridging oxygen atom (e.g., Eggler and Rosenhauer 1978). The equilibrium constant for this reaction would then predict that the carbonate/CO_2 ratio should increase linearly with the activity of NBO in the melt or glass. However, for a given glass composition, the carbonate/CO_2 ratio should be independent of the bulk CO_2 concentration, which agrees with observation if glasses are produced under otherwise identical conditions. Note that the above equation also implies that a non-bridging oxygen atom belonging to some tetrahedrally coordinated ion such as Si^{4+} or Al^{3+} is being incorporated into the carbonate group, that is, the carbonate group may become attached to the silicate network of the glass or melt. This idea is adopted in many speciation models (e.g., Brooker et al. 2001b) and appears to be consistent with the result from molecular dynamics (Guillot and Sator 2011).

The degree of polymerization or the NBO/T ratio is, however, certainly not the only parameter that controls the carbonate/CO_2 ratio in glasses. Brooker et al. (1999) studied glasses along the join $NaAlO_2$-SiO_2, which should all be fully polymerized (NBO/T = 0).

However, while there is mostly molecular CO_2 and very little carbonate in albite ($NaAlSi_3O_8$) glass, carbonate is prominent and molecular CO_2 nearly absent in nepheline ($NaAlSiO_4$) glass. Moreover, replacing 2 Na^+ by 1 Ca^{2+} appears to strongly enhance carbonate at the expense of molecular CO_2 (Brooker et al. 2001b).

The nature of the carbonate groups. The splitting of the ν_3 asymmetric stretching vibration of carbonate in glasses as seen in infrared spectra (Fig. 13) suggests that the carbonate group is in some asymmetric environment. For most natural glass compositions (basalt, andesite, phonolite), the two band components are separated by 80-100 cm^{-1} (Brooker et al. 2001b), similar to the splitting observed in glasses of the albite-diopside join in Figure 13. However, a wide range of splittings $\Delta\nu_3$ have been observed in different synthetic glass systems and sometimes several distinct carbonate species coexist (Brooker et al. 1999, 2001b). (1) Very large splittings (215-295 cm^{-1}) can be observed in fully polymerized sodium aluminosilicate melts, e.g., along the albite-nepheline join. (2) In alkali silicate glasses, two carbonate groups may coexist, one with $\Delta\nu_3 \approx 300$ cm^{-1} and one with $\Delta\nu_3 \approx 35$ cm^{-1}. (3) Adding small amounts of Mg and particularly of Ca to fully polymerized glasses causes an abrupt change in the environment of the carbonate group. For Mg, new bands with $\Delta\nu_3 \approx 168$ cm^{-1} appear, while for Ca, bands with $\Delta\nu_3 \approx 80$ cm^{-1}, similar to those observed in natural glasses, become predominant in the spectra.

The observation that the splitting of the ν_3 bands of the carbonate group in natural glass composition is very similar to that observed upon addition of Ca to various base compositions strongly suggest that in these glasses, the carbonate ion is somehow associated with the Ca^{2+} ion. Moreover, the fact that the corresponding bands appear already when a small amount of Ca^{2+} is added implies that the association between Ca^{2+} and carbonate in the glass is very stable. Brooker et al. (2001b) suggested that the carbonate in Ca-bearing systems with a typical $\Delta\nu_3 \approx 80$ cm^{-1} is related to a carbonate group close to a Ca^{2+} ion and attached via a non-bridging oxygen atom to a silicate or aluminate tetrahedron. The carbonate groups with very large $\Delta\nu_3$ in fully polymerized sodium aluminosilicate systems may form bridges between two tetrahedra, while some peralkaline glasses, where $\Delta\nu_3$ is negligible, may contain carbonate groups not attached to any NBO and surrounded only by alkali ions.

The band assignments made above are plausible and in general agreement with predictions from molecular orbital calculations (Kubicki and Stolper 1995). However, the observed $\Delta\nu_3$ strictly is only a measure of the distortion in the environment of the carbonate group and by itself does not imply chemical bonding to a specific ion. Similar splittings as observed in glasses can sometimes be seen in crystalline carbonates. In simple, calcite-structure carbonates, there is only one ν_3 band (at 1435 cm^{-1} for calcite and at 1450 cm^{-1} for magnesite; White 1974). Small splittings are seen in alkali carbonates, such as Na_2CO_3 (1413 and 1425 cm^{-1}; White 1974), while much larger splittings occur in double carbonates such as shortite $Na_2Ca_2(CO_3)_3$. Shortite contains two crystallographically distinct carbonate groups (Dickens et al. 1971), yielding a total of four infrared bands at 1522, 1481, 1453, and 1410 cm^{-1} (White 1974). Both carbonate groups in the shortite structure are bonded to two Ca ions and one Na ion in the plane of the carbonate group and the resulting asymmetry in the environment is believed to cause the splitting of ν_3 (Taylor 1990). A relatively large splitting of the carbonate band ($\Delta\nu_3 \approx 100$ cm^{-1}) has also been observed for scapolite, although the carbonate group in this mineral is not attached to a silicate tetrahedron (Papike and Stephenson 1966).

In some early studies, changes in the Si-O stretching region of the Raman spectra upon dissolution of CO_2 in the glass were interpreted in terms of CO_2 solubility mechanisms. Mysen and Virgo (1980a,b) suggested that CO_2 depolymerizes albite and anorthite glasses, while it polymerizes diopside and $NaCaAlSi_2O_7$ glass. However, the changes in the Raman spectra are generally very subtle (Fig. 14) and the models for the deconvolution and assignment of individual band components are not unique. Furthermore, while it is plausible that carbonate

is associated with some cations, in particular with Ca^{2+} in Ca-bearing glasses, there is little spectroscopic evidence that would suggest the formation of cation-carbonate complexes, in the sense of stable, molecule-like units. Indeed, the position and splitting of carbonate bands observed in most glasses is well within the range of parameters observed for crystalline carbonates or minerals such as scapolite (see above), where carbonate is coordinated by some alkali or alkaline earth cations, but where discrete molecule-like carbonate-cation complexes do not exist. Molecular dynamics studies of CO_2 in silicate melts also failed to find evidence for such complexes (Guillot and Sator 2011).

The nature of molecular CO_2 dissolved in silicate glass. The antiymmetric stretching frequency of molecular CO_2 in glasses (near 2350 cm^{-1}, see also Fig. 13) is very close to the values observed to gaseous CO_2 (2348 cm^{-1}), implying a generally similar geometry of the molecule and only weak interactions with the host glass matrix. This is consistent with the very slight difference in ^{13}C chemical shift between pure CO_2 gas (124.2 ppm) and CO_2 in silicate glasses (125 ppm; Kohn et al. 1991; Brooker et al. 1999; Morizet et al. 2002). The CO_2 band observed in the glass, however, does not show any rotational fine structure, implying that the molecule cannot rotate freely. Also, the intensity ratio of the Fermi diade in the Raman spectra of the glasses is very different from gaseous CO_2 (Brooker et al. 1999) and the infrared extinction coefficients vary considerably with glass composition (Table 4). These observations suggest that there must be some, although weak, interaction between the CO_2 molecule and the matrix. Molecular orbital calculations suggest that the CO_2 molecule in silicate glasses has a slightly bent geometry, with a O-C-O angle of 168-179° (Tossel 1995; Kubicki and Stolper 1995). The molecular dynamics model of Guillot and Sator (2011) suggest that in silicate melts, the CO_2 molecules are not randomly distributed through the melt, but preferentially located near oxygen atoms, with a preference for non-bridging oxygen atoms.

Other carbon species in glasses. Carbon monoxide (CO) has sometimes been detected as a minor species in glasses prepared under reducing conditions. In the ^{13}C NMR spectra (Fig. 15b), it may occur as a minor peak at 183 ppm (Brooker et al. 1999). Under extremely reduced conditions, carbon may be present in atomic or amorphous form (Kadik et al. 2004) or even in the form of CH_4 species (Kadik et al. 2006, 2010; Mysen et al. 2009).

Equilibrium carbon speciation in silicate melts

Annealing experiments. Brey (1976) noted that infrared spectra of quenched glasses show only carbonate bands for depolymerized compositions, while in albite glass molecular CO_2 occurs. Brey (1976) suggested that in the albite melts at high temperature, CO_2 was also dissolved as carbonate and reverted to molecular CO_2 upon quenching. Stolper et al. (1987) noted that the ratio of carbonate to molecular CO_2 in quenched albite glasses appeared to depend slightly on run temperature, with higher temperatures shifting the equilibrium towards carbonate. However, the structure of glasses represents only the structure of the melt at the glass transformation temperature T_g. Above T_g, structural relaxation is so fast that it cannot be preserved during quenching. Accordingly, it is unlikely that variations in melt structure as function of run temperatures could be directly observed in quenched glasses. Nowak et al. (2003) later suggested that the variations observed by Stolper et al. (1987) may be the result of subtle variations in water content that affect the glass transformation temperature.

Direct evidence for the true temperature dependence of carbon species was provided by Morizet et al. (2001) and Nowak et al. (2003), who carried out annealing experiments of CO_2-bearing glasses below the glass transformation temperature. In both studies, it was observed that increasing annealing temperature shifts the equilibrium towards molecular CO_2 and not towards carbonate, as previously assumed. These studies also indicate that CO_2 speciation is decoupled from the relaxation of the bulk glass structure, i.e., the equilibrium between molecular CO_2 and carbonate can be reset at temperatures where relaxation of the bulk glass structure is not expected to occur.

Morizet et al. (2001) annealed CO_2-bearing, fully polymerized jadeite glasses at 400 to 575 °C in a 1-atm furnace for variable run durations and quenched the samples rapidly to room temperature. They found that in the experiment at 575 °C, the ratio of molecular CO_2 to carbonate first increases sharply for annealing times of less than one hour and then apparently reached some equilibrium value, while at 400 and 450 °C, the CO_2/carbonate ratio decreased. From their data, they concluded that the equilibrium between molecular CO_2 and carbonate shifts towards molecular CO_2 at high temperature. For jadeite glass and melt, they estimated standard state thermodynamic data for the speciation reaction (10) of $\Delta H = -17$ (+4/−8) kJ mol^{-1} and $\Delta S = -24$ (+6/−9) J mol^{-1} K^{-1}. Morizet et al. (2001) also give kinetic data for the rate constants of the interconversion between CO_2 and carbonate. For the forward reaction (10) they find an activation energy of 68 (+3/−31) kJ mol^{-1} and for the reverse reaction of 86 (+1 /−69) kJ mol^{-1}.

The annealing experiments of Morizet et al. (2001) were carried out at 1 atm, where CO_2 should ultimately exsolve from the glass. Therefore, it is conceivable that they do not fully represent (metastable) thermodynamic equilibrium. However, Nowak et al. (2003) carried out similar annealing experiments under pressure in an internally-heated gas pressure vessel using albite and dacite glasses and obtained results that broadly agree with those of Morizet et al. (2001). Some of the results of Nowak et al. (2003) are shown in Figure 16. Annealing CO_2-bearing albite and dacite glass below the glass transformation temperature appears to reset the equilibrium between molecular CO_2 and carbonate such that with increasing temperature, molecular CO_2 becomes more abundant and carbonate decreases. Notably, Nowak et al. (2003) could also show reversibility of the CO_2 speciation equilibrium, that is, the speciation observed in a dacite glass at 879 K was the same for glasses first annealed at 973 K or at 789 K. For the fully polymerized albite glass, they obtained $\Delta H = -12$ (±3) kJ mol^{-1} and $\Delta S =$

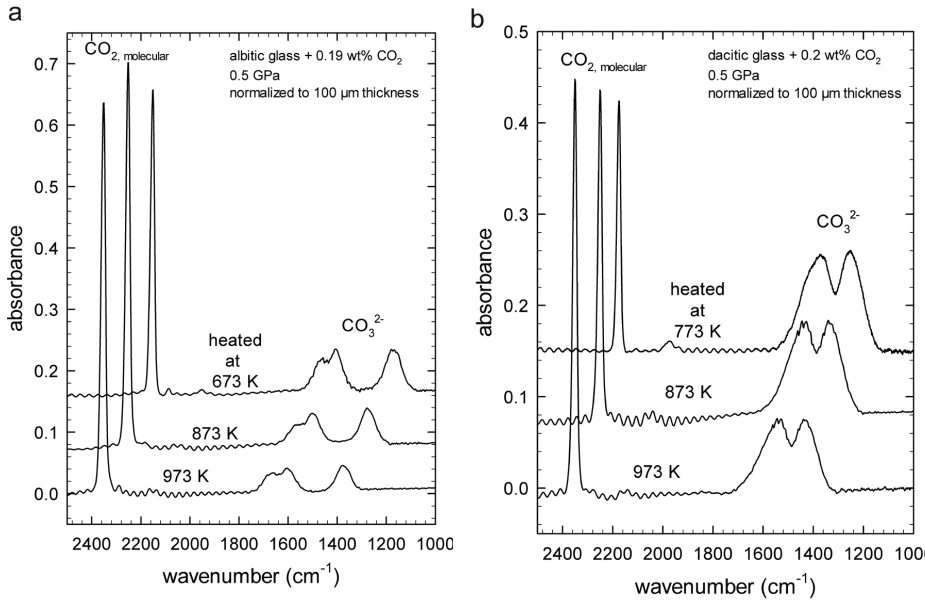

Figure 16. Infrared spectra of CO_2-bearing (a) albite and (b) dacite glasses annealed at different temperatures. Note the increase of molecular CO_2 and the decrease of carbonate with increasing temperature. Spectra courtesy of Marcus Nowak.

−23 (±2) J mol^{-1} K^{-1}, similar to the data for the fully polymerized jadeite glass reported by Morizet et al. (2001). However, for the slightly depolymerized dacite glass, they observed a significantly higher reaction enthalpy (ΔH = −29 (±3) kJ mol^{-1}; ΔS = −32 (±2) J mol^{-1} K^{-1}).

In situ high-temperature FTIR spectroscopy. Direct, *in situ* infrared spectroscopic measurements of CO_2 speciation in a range of silicate melts were reported by Konschak (2008) and by Konschak and Keppler (2009). These experiments are very difficult, as they require temperatures in excess of 1000 °C, which is at the limit of the externally-heated diamond anvil cells used for the measurements. Moreover, blackbody emission from the cell and from the sample becomes so strong in the mid-infrared region at high temperatures that spectra cannot be measured with a conventional infrared source anymore; a synchrotron infrared source is required. Despite these experimental difficulties, however, the results obtained by these *in situ* studies are in very good agreement with the annealing experiments by Morizet et al. (2001) and by Nowak et al. (2003). With increasing temperature, equilibrium (10) in the melt shifts towards molecular CO_2 and the enthalpy of the reaction increases with the depolymerization of the melt.

Figure 17 shows typical high-temperature FTIR spectra of CO_2-bearing phonolite glass as measured in an externally heated diamond anvil cell. Up to the glass transformation temperature of 700 °C, the absorbances of both the molecular CO_2 and of the carbonate decrease. This effect is due to a reduced population of the vibrational ground state with increasing temperature and can be quantitatively modeled by a Boltzmann distribution (Konschak 2008). Beyond the glass transformation temperature, however, the intensity of the band of molecular CO_2 increases again while the carbonate band nearly vanishes, indicating a conversion of carbonate to molecular CO_2 with increasing temperature. If these data are converted to species concentrations, the equilibrium constant for reaction (10) may be calculated (Fig. 18). For dacite melt, these measurements yield ΔH = −42 (±12) kJ mol^{-1} and ΔS = −38 (±14) J mol^{-1} K^{-1}, within error quite comparable to the value reported by Nowak et al. (2003) for annealing experiments on dacite glasses of the same composition (NBO/T = 0.09). The somewhat higher value for the enthalpy may either be a pressure effect or it may indicate that annealing below the glass transformation temperature does not completely relax CO_2 speciation. For a phonolite melt (NBO/T = 0.14), Konschak (2008) obtained ΔH = −65 (±20) kJ mol^{-1}and ΔS = −51 (±20) J mol^{-1} K^{-1}. These data, together with those of Morizet et al. (2001) and Nowak et al. (2003) indicate a systematic increase of ΔH of reaction (10) with NBO/T (Fig. 19). By linear regression of ΔS and ΔH, as a function of NBO/T, Konschak (2008) constructed a model that predicts the equilibrium between molecular CO_2 and carbonate over a wide range of temperatures and compositions. As shown in Figure 20, the equilibrium constant, which for a model of ideal mixing of oxygen atoms is virtually identical with the molar carbonate/molecular CO_2 ratio, is strongly dependent on temperature. At 1000-1200 °C, there is indeed a major difference in CO_2 speciation between rhyolite (NBO/T ≈ 0) and basalt (NBO/T = 0.5-1), with carbonate prevailing in low-temperature basaltic melts. However, at higher temperatures near 1500 °C, this difference in speciation nearly disappears and molecular CO_2 is the predominant carbon species. This implies that the dependence of CO_2 solubility on melt composition should become less pronounced at higher temperatures, in general agreement with measurements and results from molecular dynamics simulations (Fig. 4).

The results from annealing experiments and from *in situ* measurements outlined here are in good agreement with the recent molecular dynamics simulation by Guillot and Sator (2011). They found that molecular CO_2 is present even in mafic and ultramafic melts at superliquidus conditions and the fraction of total carbon dissolved as molecular CO_2 increases with temperature, while it decreases with pressure. Molecular CO_2 is only loosely associated with melt structure (Fig. 21a). On the other hand, the carbonate groups are preferentially associated with non-bridging oxygen atoms while the association of CO_3^{2-} with bridging oxygen is also present (Fig. 21b).

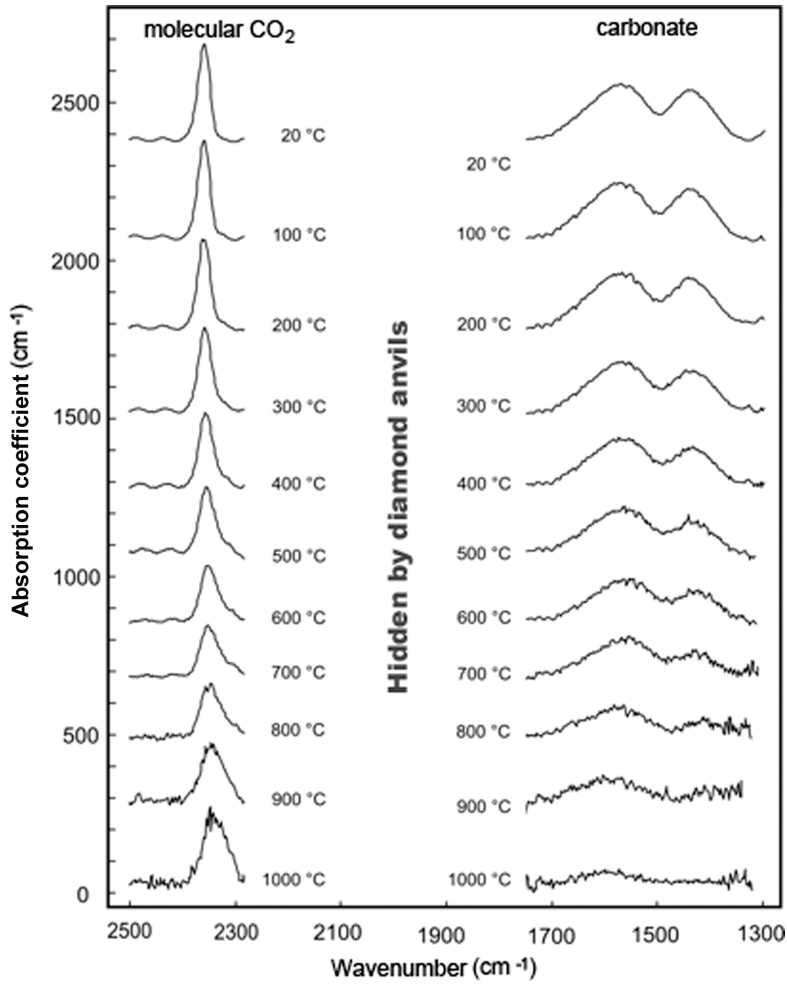

Figure 17. High-temperature *in situ* FTIR spectra of dacite melt with 1.6 wt% CO_2. Pressure increases from 5 GPa at room temperature to 14 GPa at 1000 C. Spectra were measured at the synchrotron source ANKA in Karlsruhe, Germany. After Konschak (2008).

PHYSICAL PROPERTIES OF CARBON-BEARING SILICATE MELTS

Viscosity and electrical conductivity

Brearley and Montana (1989) observed in high-pressure falling-sphere experiments that CO_2 slightly reduced the viscosity of albite melt, while the effect on sodium melilitite melt was negligible. White and Montana (1990) observed that 0.5 wt% CO_2 slightly decreases the viscosity of sanidine melt at 1.5-2 GPa and 1500 °C. Bourgue and Richet (2001) reported that the viscosity of a potassium silicate liquid with 56.9 mol% SiO_2 decreases by two orders of magnitude upon addition of 3.5 wt% CO_2 at 750 K and 1 atm. However, the effect of 1 wt% CO_2 at 1500 K on the viscosity of the same melt is almost negligible. More recently, Morizet et al. (2007) found that dissolved CO_2 has little or no effect on the glass transformation temperature of phonolite and jadeite glasses, implying a negligible effect of CO_2 on viscosity. Ni et al. (2011) found that 0.5 wt% CO_2 has virtually no effect on the electrical conductivity of basaltic

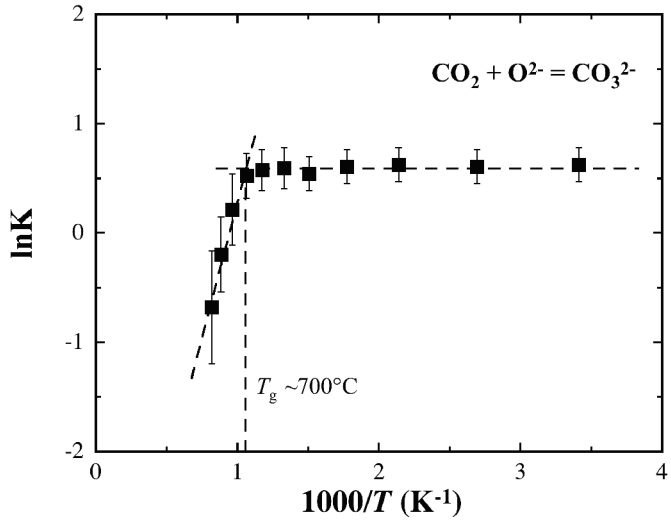

Figure 18. Temperature dependence of the equilibrium constant K of the reaction $CO_2 + O^{2-} = CO_3^{2-}$ in dacite melt from *in situ* FTIR measurements. Below the glass tranformation temperature T_g of about 700 °C, species concentrations are unchanged (out of equilibrium due to slow reaction). From Konschak (2008).

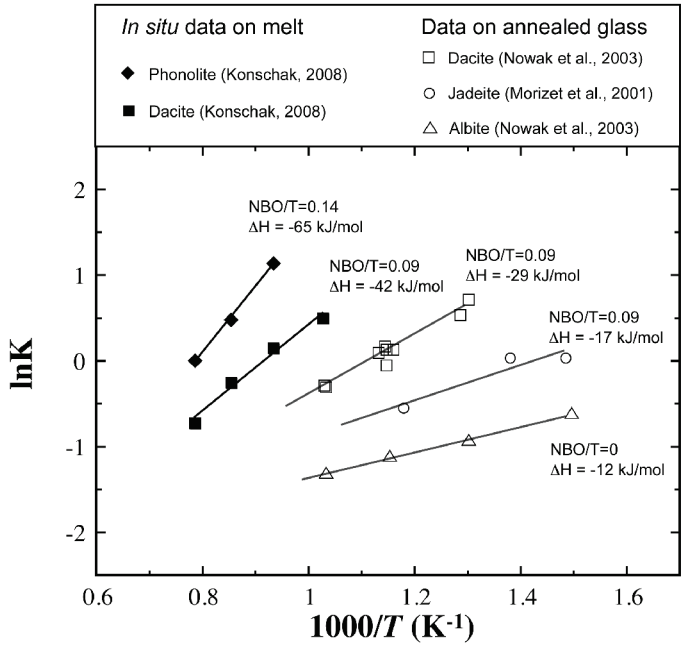

Figure 19. Temperature dependence of the equilibrium constant K of the reaction $CO_2 + O^{2-} = CO_3^{2-}$ for various melt compositions, from annealing experiments (open symbols) and *in situ* measurements (solid symbols). Parameter NBO/T and reaction enthalpy (ΔH) are indicated for each composition. From Konschak (2008).

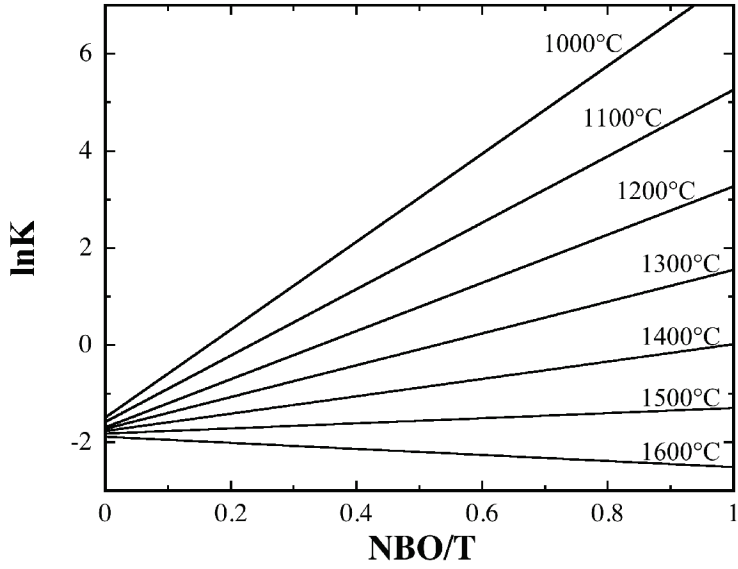

Figure 20. Equilibrium constant K of the reaction $CO_2 + O^{2-} = CO_3^{2-}$ in silicate melts for various temperatures and melt compositions as represented by the NBO/T parameter. For a model of ideal mixing of oxygen atoms, this constant nearly equals the molar carbonate/CO_2 ratio. Curves are calculated from a linear relationship between ΔS and ΔH of the reaction and NBO/T. From Konschak (2008).

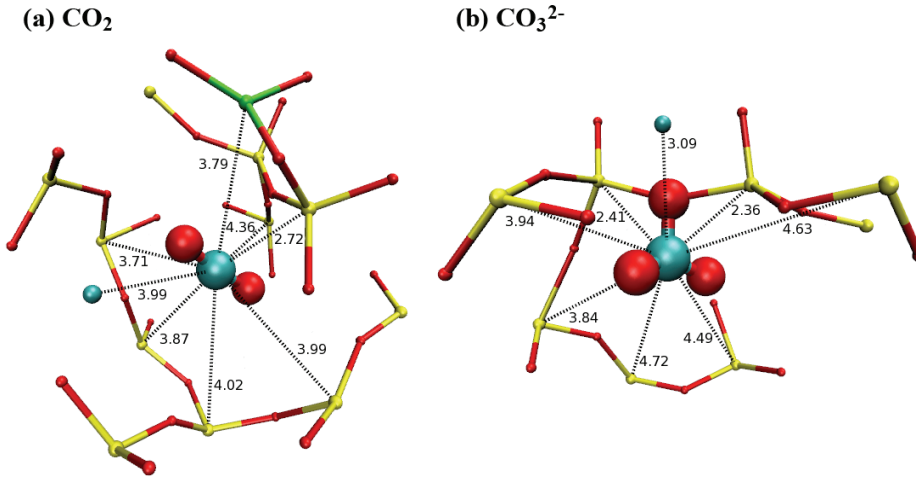

Figure 21. Snapshots of representative (a) molecular CO_2 and (b) carbonate group dissolved in basalt melt at 2273 K and 2.0 GPa from molecular dynamics simulation. Carbon atoms are the big blue balls, oxygen atoms are in red, silicon atoms are in yellow, aluminum atom is in green, and Ca atoms are the small blue balls. The numbers indicate carbon-cation distances in angstroms (only those cations < 5 angstroms away from the carbon atom are shown). Courtesy of Bertrand Guillot.

melts. The latter observation is in line with evidence from *in situ* spectroscopy (Konschak 2008) and molecular dynamics calculations (Guillot and Sator 2011) suggesting that molecular CO_2 becomes increasingly abundant with the rise of temperature. Generally, the effect of CO_2 on the transport properties of silicate melts is likely negligible, except perhaps for melts containing several wt% CO_2.

Density and molar volume

The dissolution of a light component such as CO_2 in a silicate melt will reduce density. At low pressures, this effect will be small due to the low bulk solubility of CO_2 in most melts. However, it may become very significant at deep mantle pressures. Using the sink-float method, Ghosh et al. (2007) determined the density of a basaltic melt with 5 wt% CO_2 at 2575 K and 19.5 GPa. From this measurement they derived a partial molar volume of CO_2 of 21.0 ± 1.0 cm^3/mol. Liu and Lange (2003) measured the partial molar volume of $CaCO_3$ in carbonate melts at 1 atm and obtained a partial molar volume of CO_2 in carbonate melts of 25.8 cm^3/mol. They estimated that the partial molar volume of CO_2 in alkaline, strongly depolymerized silicate melts should be 19 cm^3/mol or larger, assuming that CO_2 is dissolved in these melts as carbonate species similar to those occurring in carbonatite melts. Bourgue and Richet (2001) measured a partial molar volume of CO_2 of 25.6 ± 0.8 cm^3/mol in potassium silicate glasses at room temperature and observed that the presence of CO_2 has no effect on the thermal expansion coefficient. The thermodynamic analysis of the pressure dependence of CO_2 solubility in silicate melts suggests molar volumes in the order of 21-29 cm^3/mol (Lange 1994). These data are in broad agreement with the molecular dynamics simulations of Guillot and Sator (2011).

Diffusivity of carbon

The diffusion of carbon component in silicate melts has recently been reviewed by Zhang et al. (2007) and Zhang and Ni (2010), to which the readers are directed for a thorough discussion of the relevant studies before 2007. Here we first give a short summary largely based on Zhang and Ni (2010), which is then followed by an introduction of more recent developments. The early ^{14}C tracer diffusivity data by Watson (1991) and Watson et al. (1982) obtained by β-track autoradiography probably contained large errors because (a) β-track autoradiography cannot measure accurate carbon concentration (see the section on carbon solubility in this review); and more importantly (b) the β-particle range (in the order of 100 μm) turns out to be much higher than originally expected (i.e., the measured profiles carry significant broadening effects), as pointed out by Mungall (2002). All the later studies investigate CO_2 chemical transport and measure diffusion profiles with the more reliable FTIR microspectroscopy (Table 5). One important finding from these studies is that CO_2 diffusivity does not depend much on melt composition despite the fact that the speciation of CO_2 component can be very different (e.g., a higher fraction of molecular CO_2 in rhyolite melt than in basalt melt). Assuming the diffusion is dominated by molecular CO_2 (neutral and smaller in size), Nowak et al. (2004) attributed the weak compositional dependence to increasing molecular CO_2 diffusivity from rhyolite melt to basalt melt combined with decreasing proportion of molecular CO_2 (i.e., these two effects approximately cancel each other). Because of the scarcity of CO_2 diffusivity data, the similarity between Ar diffusivity and CO_2 diffusivity is exploited by Zhang et al. (2007) to derive the following model for apparent total CO_2 diffusivity (as well as Ar diffusivity) in rhyolite to basalt melts:

$$\ln D_{\text{total CO}_2} = -13.99 - \frac{17367 + 1944.8P}{T} + \frac{(855.2 + 271.2P)}{T} C_{\text{H}_2\text{O}} \quad (11)$$

where D is total CO_2 diffusivity in m^2/s (note that this total CO_2 diffusivity is different from molecular CO_2 diffusivity), T is absolute temperature, P is pressure in GPa, and C_{H_2O} is the total dissolved H_2O in wt%. This model, applicable within 673-1773 K, 0-1.5 GPa, and 0-5

Table 5. Studies on carbon diffusion in silicate melts

Year	Authors	Melt	Species	*T* (°C)	*P* (bar)	Analytical Method
Data						
1982	Watson et al.	SNA*, Haplobasalt	^{14}C	800-1500	500-18000	β-track mapping
1991	Watson	Rhyolite, Dacite	^{14}C	800-1100	10000	β-track mapping
1990	Fogel & Rutherford	Rhyolite	CO_2	1050	1000-2490	FTIR
1991	Zhang & Stolper	Basalt	CO_2	1300	10000	FTIR
1993	Blank	Rhyolite	CO_2	450-1050	500-1050	FTIR
2002	Sierralta et al.	Albite, Albite + Na_2O	CO_2	1250	5000	FTIR
2003	Liu	Dacite	CO_2	638	970	FTIR
2004	Nowak et al.	Rhyolite, Dacite, Andesite, Basalt Hawaiite	CO_2	1350	5000	FTIR
2005	Baker et al.	Trachyte	CO_2	1100-1300	10000-12000	FTIR
2010	Spickenbom et al.	SNA*	CO_2	1100-1350	5000	FTIR
2011	Guillot & Sator	Rhyolite, Basalt, Kimberlite	CO_2	1200-2000	20000-100000	Molecular dynamics
Model						
2007	Zhang et al.	Rhyolite to basalt	CO_2	500-1500	0-10000	

* SNA means SiO_2-Na_2O-Al_2O_3 melts.

wt% H_2O, predicts a positive H_2O effect and a negative pressure effect. It also implies that CO_2 concentration has no effect on CO_2 diffusivity, in contrast with the rapid increase of H_2O diffusivity with increasing H_2O concentration (Shaw 1974; Ni and Zhang 2008; Ni et al. 2009a,b).

In the last couple of years two new studies on CO_2 diffusion in silicate melts have been published, one experimental and the other computational. Spickenbom et al. (2010) showed that CO_2 diffusivity varies insignificantly for $Ab_{70}Qz_{30}$ melt to jadeite melt, but it increases by about a factor of 3 from albite melt to a soda-rich melt with 63.95 wt% SiO_2, 18.65 wt% Al_2O_3, and 17.4 wt% Na_2O (Fig. 22a), in accordance with Sierralta et al. (2002). Guillot and Sator (2011) performed the first molecular dynamics simulations to obtain CO_2 diffusivity at 2-10 GPa and 1473-2273 K from the mean square displacements of carbon atoms. They also found that CO_2 diffusivity increases notably with the degree of melt depolymerization (to a lesser extent from rhyolite melt to basalt melt than from basalt melt to kimberlite melt), as shown in Figure 22b using NBO/T as the index for the degree of melt depolymerization. Furthermore, their computed molecular CO_2 diffusivities support the explanation by Nowak et al. (2004) for the limited variation of total CO_2 diffusivity from rhyolite melt to basalt melt. One major difference between Guillot and Sator (2011) and the experimental studies is about the diffusivity of CO_3^{2-}. At 2273 K and 2.0 GPa, they found that CO_3^{2-} diffusivity, which is comparable to oxygen diffusivity in basalt and kimberlite melts, is lower than molecular CO_2 diffusivity by only a factor of 2-3, whereas previously CO_3^{2-} diffusivity was always assumed to be negligible (Nowak et al. 2004). However, Guillot and Sator (2011) appear to have overestimated total CO_2 diffusivities by roughly one order of magnitude.

FUTURE DIRECTIONS

After decades of experimental studies, we now have a reasonably good understanding of carbon solubility and speciation in silicate melts in Earth's crust and uppermost mantle. However, experimental data on the behavior of carbon in melts at the higher pressure regimes of the deeper upper mantle, the transition zone, and the lower mantle are lacking. An interesting, yet unexplored possibility is the conceivable occurrence of complete miscibility between CO_2 and alkaline silicate melts at very high pressures and temperatures. The behavior of carbon under reducing conditions is generally poorly explored. Moreover, there are no data on carbon solubility in peridotitic melts, and in particular in peridotitic melts under reducing conditions, which would be essential for understanding the behavior of carbon in a magma ocean. Such data would be essential for constraining the initial distribution of carbon in Earth. Many of these problems will likely require molecular dynamic simulations or a further advancement in *in situ* experimental methods for studying carbon speciation and solubility (Oganov et al. 2013). In Earth's upper mantle, carbon dioxide in general appears to have less influence on the physical properties of silicate melts than water, but its effects need to be better quantified. How reduced carbon species may modify melt properties also needs to be examined, and will provide additional challenges to experimental and theoretical geoscientists.

ACKNOWLEDGMENTS

We thank Zhigang Zhang for the program calculating CO_2 fugacity of C-O-H fluids, Bertrand Guillot for the microscopic pictures of carbon species, and Paolo Papale for discussion. A formal review by David Dobson has improved the manuscript.

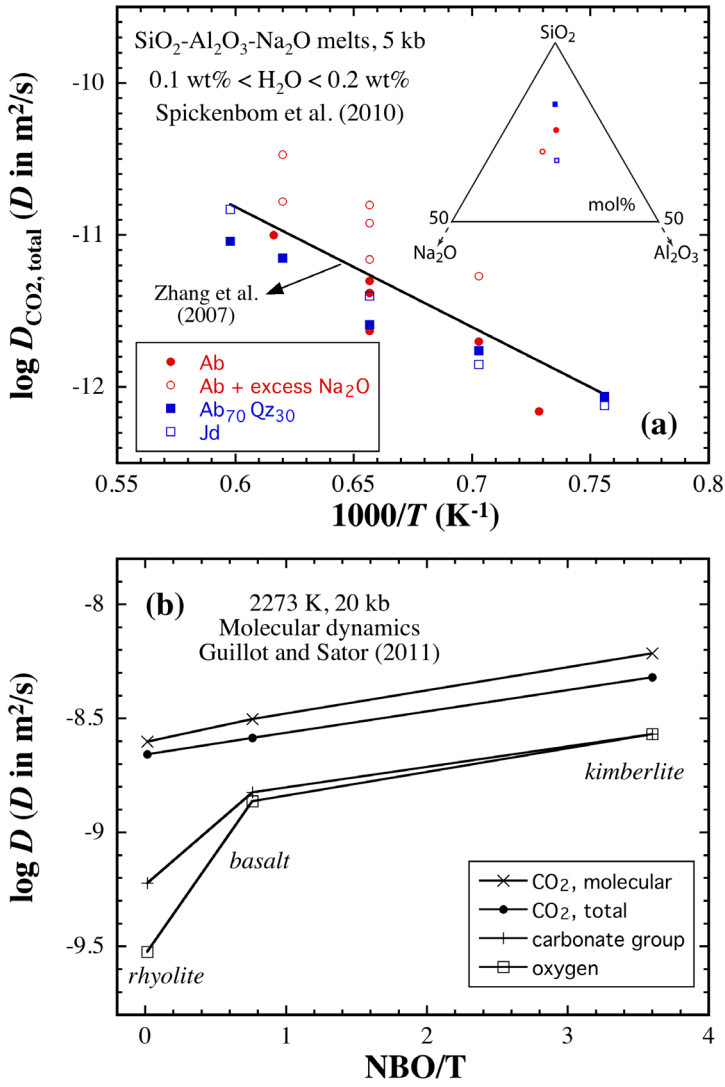

Figure 22. (a) Experimental total CO_2 diffusivity at 0.5 GPa in four anhydrous (H_2O ranging from 0.1 to 0.2 wt%) SiO_2-Al_2O_3-Na_2O melts with the inlet showing the loci of melts in compositional space. Modified after Spickenbom et al. (2010). Calculations using the composition-independent model of Zhang et al. (2007) at 0.15 wt% H_2O are shown for comparison (solid line). (b) Molecular dynamics-derived diffusivity of total CO_2, molecular CO_2, CO_3^{2-}, and oxygen versus NBO/T of three melts at 2273 K and 2.0 GPa. After Guillot and Sator (2011).

REFERENCES

Baker DR, Freda C, Brooker RA, Scarlato P (2005) Volatile diffusion in silicate melts and its effects on melt inclusions. Ann Geophys 48:699-717

Ballhaus C (1995) Is the upper mantle metal-saturated? Earth Planet Sci Lett 132:75-86

Beerling D (2002) CO_2 and the end-Triassic mass extinction. Nature 415:386-387

Behrens H, Misiti V, Freda C, Vetere F, Botcharnikov RE, Scarlato P (2009) Solubility of H_2O and CO_2 in ultrapotassic melts at 1200 and 1250 °C and pressure from 50 to 500 MPa. Am Mineral 94:105-120

Behrens H, Ohlhorst S, Holtz F, Champenois M (2004a) CO_2 solubility in dacitic melts equilibrated with H_2O-CO_2 fluids: implications for modeling the solubility of CO_2 in silicic melts. Geochim Cosmochim Acta 68:4687-4703

Behrens H, Tamic N, Holtz F (2004b) Determination of the molar absorption coefficient for the infrared absorption band of CO_2 in rhyolitic glasses. Am Mineral 89:301-306

Berner RA (1994) 3GEOCARB II: A revised model for atmospheric CO_2 over Phanerozoic time. Am J Sci 294:56-91

Blank JG (1993) An experimental investigation of the behavior of carbon dioxide in rhyolitic melt. PhD dissertation, California Institute of Technology, Pasadena, CA

Blank JG, Brooker RA (1994) Experimental studies of carbon dioxide in silicate melts: solubility, speciation, and stable carbon isotope behavior. Rev Mineral 30:157-186

Botcharnikov RE, Behrens H, Holtz F (2006) Solubility and speciation of C-O-H fluids in andesitic melt at *T*=1100-1300 °C and *P*=200 and 500 MPa. Chem Geol 229:125-143

Botcharnikov RE, Freise M, Holtz F, Behrens H (2005) Solubility of C-O-H mixtures in natural melts: new experimental data and application range of recent models. Ann Geophys 48:633-646

Botcharnikov RE, Holtz F, Behrens H (2007) The effect of CO_2 on the solubility of H_2O-Cl fluids in andesitic melt. Eur J Mineral 19:671-680

Bourgue E, Richet P (2001) The effects of dissolved CO_2 on the density and viscosity of silicate melts: a preliminary study. Earth Planet Sci Lett 193:57-68

Brearley M, Montana A (1989) The effect of CO_2 on the viscosity of silicate liquids at high pressure. Geochim Cosmochim Acta 53:2609-2616

Brey G (1976) CO_2 solubility and solubility mechanisms in silicate melts at high pressures. Contrib Mineral Petrol 57: 215-221

Brey G, Green DH (1975) The role of CO_2 in the genesis of olivine melilitite. Contrib Mineral Petrol 49:93-103

Brooker RA, Kohn SC, Holloway JR, McMillan PF (2001a) Structural controls on the solubility of CO_2 in silicate melts. Part I: bulk solubility data. Chem Geol 174:225-239

Brooker RA, Kohn SC, Holloway JR, McMillan PF (2001b) Structural controls on the solubility of CO_2 in silicate melts. Part II: IR characteristics of carbonate groups in silicate glasses. Chem Geol 174:241-254

Brooker RA, Kohn SC, Holloway JR, McMillan PF, Carroll MR (1999) Solubility, speciation and dissolution mechanisms for CO_2 in melts on the $NaAlO_2$-SiO_2 join. Geochim Cosmochim Acta 63:3549-3565

Chase MW Jr (1998) NIST-JANAF Thermochemical Tables. Fourth Edition. J Phys Chem Ref Data, Monograph 9

Dasgupta R, Hirschmann, MM (2010) The deep carbon cycle and melting in Earth's interior. Earth Planet Sci Lett 298:1-13

Dickens B, Hyman A, Brown WE (1971) Crystal structure of $Ca_2Na_2(CO_3)_3$ (shortite). J Res Nat Bur Stand 75A:129-135

Dixon JE (1997) Degassing of alkalic basalts. Am Mineral 82:368-378

Dixon JE, Pan V (1995) Determination of the molar absorptivity of dissolved carbonate in basanitic glass. Am Mineral 80:1339-1342

Dixon JE, Stolper EM, Holloway JR (1995) An experimental study of water and carbon dioxide solubilites in Mid-Ocean Ridge basaltic liquids. Part I: calibration and solubility models. J Petrol 36:1607-1631

Duan Z, Moller N, Weare JH (1992) An equation of state for the CH_4-CO_2-H_2O system: I. Pure systems from 0 to 1000 °C and 0 to 8000 bar. Geochim Cosmochim Acta 56:2605-2617

Duan Z, Zhang Z (2006) Equation of state of the H_2O, CO_2, and H_2O-CO_2 systems up to 10 GPa and 2573.15 K: molecular dynamics simulations with *ab inito* potential surface. Geochim Cosmochim Acta 70:2311-2324

Eggler DH, Mysen BO, Hoering TC, Holloway JR (1979) The solubility of carbon monoxide in silicate melts at high pressures and its effect on silicate phase relations. Earth Planet Sci Lett 43:321-330

Eggler DH, Rosenhauer M (1978) Carbon dioxide in silicate melts: II. Solubilities of CO_2 and H_2O in $CaMgSi_2O_6$ (diopside) liquids and vapors at pressures to 40 kbar. Am J Sci 278:64-94

Fine G, Stolper E (1985) The speciation of carbon dioxide in sodium aluminosilicate glasses. Contrib Mineral Petrol 91:105-121

Fine G, Stolper E (1986) Dissolved carbon dioxide in basaltic glasses: concentrations and speciation. Earth Planet Sci Lett 76:263-278

Fogel RA, Rutherford MJ (1990) The solubility of carbon dioxide in rhyolitic melts: a quantitative FTIR study. Am Mineral 75:1311-1326

Frost DJ, McCammon CA (2008). The redox state of the Earth's mantle. Ann Rev Earth Planet Sci 36:389-420

Ghosh S, Ohtani E, Litasov K, Suzuki A, Sakamaki T (2007) Stability of carbonated magma at the base of Earth's upper mantle. Geophys Res Lett 34:L22312, doi:10.1029/2007GL031349

Gottschalk M (2007) Equations of state for complex fluids. Rev Mineral Geochem 65:49-97
Guillot B, Sator N (2011) Carbon dioxide in silicate melts: a molecular dynamics simulation study. Geochim Cosmochim Acta 75:1829-1857
Hoffman PF, Kaufmann AJ, Halverson GP, Schrag DP (1998) A Neoproterozoic snowball Earth. Science 281:1342-1346
Holloway JR (1976) Fluids in the evolution of granitic magmas: consequences of finite CO_2 solubility. Geol Soc Am Bull 87:1513-1518
Holloway JR, Blank JG (1994) Application of experimental results to C-O-H species in natural melts. Rev Mineral Geochem 30:187-230
Holloway JR, Jakobsson S (1986) Volatile solubilities in magmas: transport of volatiles from mantles to planet surfaces. J Geophys Res 91:D505-D508
Iacono-Marziano G, Morizet Y, Le Trong E, Gaillard F (2012) New experimental data and semi-empirical parameterization of H_2O-CO_2 solubility in mafic melts. Geochim Cosmochim Acta 97:1-23
Jakobsson S (1997) Solubility of water and carbon dioxide in an icelandite at 1400 °C and 10 kilobars. Contrib Mineral Petrol 127:129-135
Jakobsson S, Holloway JR (1986) Crystal-liquid experiments in the presence of a C-O-H fluid buffered by graphite + iron + wustite: experimental method and near-liquidus relations in basanite. J Volcanol Geotherm Res 29:265-291
Jendrzejewski N, Trull TW, Pineau F, Javoy M (1997) Carbon solubility in Mid-Ocean Ridge basaltic melt at low pressures (250-1950 bar). Chem Geol 138:81-92
Kadik AA, Kurovskaya NA, Ignat'ev YA, Kononkova NN, Koltashev VV (2010) Influence of oxygen fugacity on the solubility of carbon and hydrogen in FeO-Na_2O-SiO_2-Al_2O_3 melts in equilibrium with liquid iron at 1.5 GPa and 1400 °C. Geochem Int 48:953-960
Kadik AA, Kurovskaya NA, Ignat'ev YA, Kononkova NN, Koltashev VV, Plotnichenko VG (2011) Influence of oxygen fugacity on the solubility of nitrogen, carbon and hydrogen in FeO-Na_2O-SiO_2-Al_2O_3 melts in equilibrium with metallic iron at 1.5 GPa and 1400 °C. Geochem Int 49:429-438
Kadik AA, Litvin YA, Koltashev VV, Kryukova EB, Plotnichenko VG (2006) Solubility of hydrogen and carbon in reduced magmas of the early Earth's mantle. Geochem Int 44:33-47
Kadik AA, Pineau F, Litvin YA, Jendrzejewski N, Martinez I, Javoy M (2004) Formation of carbon and hydrogen species in magmas at low oxygen fugacity. J Petrol 45:1297-1310
Kerrick DM, Jacobs GK (1981) A modified Redlich-Kwong equation for H_2O, CO_2, and H_2O-CO_2 mixtures at elevated pressures and temperatures. Am J Sci 281:735-767
Keshav S, Gudfinnsson GH, Presnall DC (2011) Melting phase relations of simplified carbonated peridotite at 12-26 GPa in the systems CaO-MgO-SiO_2-CO_2 and CaO-MgO-Al_2O_3-SiO_2-CO_2: highly calcic magmas in the transition zone of the Earth. J Petrol 52:2265-2291
King PL, Holloway JR (2002) CO_2 solubility and speciation in intermediate (andesitic) melts: the role of H_2O and composition. Geochim Cosmochim Acta 66:1627-1640
Kohn SC, Brooker RA, Dupree R (1991) ^{13}C MAS NMR: A method for studying CO_2 speciation in glasses. Geochim Cosmochim Acta 55:3879-3884
Konschak A (2008) CO_2 in Silikatschmelzen. Ph. D. dissertation, University of Bayreuth, Germany
Konschak A, Keppler H (2009) A model for CO_2 solubility in silicate melts. Geochim Cosmochim Acta 73:A 680
Kubicki JD, Stolper EM (1995) Structural roles of CO_2 and $[CO_3]^{2-}$ in fully polymerized, sodium aluminosilcate melts and glasses. Geochim Cosmochim Acta 59:683-698
Kump LR, Barley ME (2007) Increased subaerial volcanism and the rise of atmospheric oxygen 2.5 billion years ago. Nature 448:1033-1036
Lange RA (1994) The effect of H_2O, CO_2 and F on the density and viscosity of silicate melts. Rev Mineral 30:331-369
Lesne P, Scaillet B, Pichavant M, Beny J-M (2011) The carbon dioxide solubility in alkali basalts: an experimental study. Contrib Mineral Petrol 162:153-168
Liu Q, Lange RA (2003) New density measurements on carbonate liquids and the partial molar volume of the $CaCO_3$ component. Contrib Mineral Petrol 146:370-381
Liu Y (2003) Water in rhyolitic and dacitic melts. Ph.D. dissertation, University of Michigan
Liu Y, Zhang Y, Behrens H (2005) Solubility of H_2O in rhyolitic melts at low pressures and a new empirical model for mixed H_2O-CO_2 solubility in rhyolitic melts. J Volcanol Geotherm Res 143:219-235
Manning CE, Shock EL, Sverjensky D (2013) The chemistry of carbon in aqueous fluids at crustal and upper-mantle conditions: experimental and theoretical constraints. Rev Mineral Geochem 75:109-148
Mattey DP (1991) Carbon dioxide solubility and carbon isotope fractionation in basaltic melt. Geochim Cosmochim Acta 55:3467-3473
McCammon C (2005) The paradox of mantle redox. Science 308:807-808

Moore G (2008) Interpreting H_2O and CO_2 contents in melt inclusions: constraints from solubility experiments and modeling. Rev Mineral Geochem 69:333-361

Morizet Y, Brooker RA, Kohn SC (2002) CO_2 in haplo-phonolite melt: solubility, speciation and carbonate complexation. Geochim Cosmochim Acta 66:1809-1820

Morizet Y, Kohn SC, Brooker RA (2001) Annealing experiments on CO_2-bearing jadeite glass: an insight into the true temperature dependence of CO_2 speciation in silicate melts. Mineral Mag 65:701-707

Morizet Y, Paris M, Gaillard F, Scaillet B (2010) C-O-H fluid solubility in haplobasalt under reducing conditions: an experimental study. Chem Geol 279:1-16

Morizet, Y, Nichols ARL, Kohn SC, Brooker RA, Dingwell DB (2007) The influence of H_2O and CO_2 on the glass transition temperature: insights into the effects of volatiles on magma viscosity. Eur J Mineral 19:657-669

Mungall JE (2002) Empirical models relating viscosity and tracer diffusion in magmatic silicate melts. Geochim Cosmochim Acta 66:125-143

Mysen BO (1976) The role of volatiles in silicate melts: solubility of carbon dioxide and water in feldspar, pyroxene, and feldspathoid melts to 30 kb and 1625 °C. Am J Sci 276:969-996

Mysen BO, Arculus RJ, Eggler DH (1975) Solubility of carbon dioxide in melts of andesite, tholeiite, and olivine nephelininte composition to 30 kbar pressure. Contrib Mineral Petrol 53:227-239

Mysen BO, Eggler DH, Seitz MG, Holloway JR (1976) Carbon dioxide in silicate melts and crystals. Part I. Solubility measurements. Am J Sci 276:455-479

Mysen BO, Fogel ML, Morrill PL, Cody GD (2009) Solution behavior of reduced C-O-H volatiles in silicate melts at high pressure and temperature. Geochim Cosmochim Acta 73:1696-1710

Mysen BO, Virgo D (1980a) Solubility mechanism of carbon dioxide in silicate melts: a Raman spectroscopic study. Am Mineral 65:885-899

Mysen BO, Virgo D (1980b) The solubility behavior of CO_2 in melts on the join $NaAlSi_3O_8$-$CaAl_2Si_2O_8$-CO_2 at high pressures and temperatures: A Raman spectroscopic study. Am Mineral 65:1166-1175

Newman S, Lowenstern JB (2002) VolatileCalc: a silicate melt-H_2O-CO_2 solution model written in Visual Basic for excel. Computat Geosci 28:597-604

Ni H, Behrens H, Zhang Y (2009b) Water diffusion in dacitic melt. Geochim Cosmochim Acta 73:3642-3655

Ni H, Keppler H, Behrens H (2011) Electrical conductivity of hydrous basaltic melts: implications for partial melting in the upper mantle. Contrib Mineral Petrol 162:637-650

Ni H, Liu Y, Wang L, Zhang Y (2009a) Water speciation and diffusion in haploandesitic melts at 743-873 K and 100 MPa. Geochim Cosmochim Acta 73:3630-3641

Ni H, Zhang Y (2008) H_2O diffusion models in rhyolitic melt with new high pressure data. Chem Geol 250:68-78

Nowak M, Porbatzki D, Spickenbom K, Diedrich O (2003) Carbon dioxide speciation in silicate melts: a restart. Earth Planet Sci Lett 207:131-139

Nowak M, Schreen D, Spickenbom K (2004) Argon and CO_2 on the race track in silicate melts: a tool for the development of a CO_2 speciation and diffusion model. Geochim Cosmochim Acta 68:5127-5138

Oganov AR, Hemley RJ, Hazen RM, Jones AP (2013) Structure, bonding, and mineralogy of carbon at extreme conditions. Rev Mineral Geochem 75:47-77

Pan V, Holloway JR, Hervig RL (1991) The pressure and temperature dependence of carbon dioxide solubility in tholeiitic basalt melts. Geochim Cosmochim Acta 55:1587-1595

Paonita A, Gigli G, Gozzi D, Nuccio PM, Trigila R (2000) Investigation of the He solubility in H_2O-CO_2 bearing silicate liquids at moderate pressure: a new experimental method. Earth Planet Sci Lett 181:595-604

Papale P (1997) Modeling of the solubility of a one-component H_2O or CO_2 fluid in silicate liquids. Contrib Mineral Petrol 126:237-251

Papale P (1999) Modeling of the solubility of a two-component $H_2O + CO_2$ fluid in silicate liquids. Am Mineral 84:477-492

Papale P, Moretti R, Barbato D (2006) The compositional dependence of the saturation surface of $H_2O + CO_2$ fluids in silicate melts. Chem Geol 229:78-95

Papale P, Polacci M (1999) Role of carbon dioxide in the dynamics of magma ascent in explosive eruptions. Bull Volcanol 60:585-594

Papike JJ, Stephenson NC (1966) The crystal structure of mizzonite, a calcium- and carbonate-rich scapolite. Am Mineral 51:1014-1027

Pawley AR, Holloway JR, McMillan PF (1992) The effect of oxygen fugacity on the solubility of carbon-oxygen fluids in basaltic melt. Earth Planet Sci Lett 110:213-225

Shaw HR (1974) Diffusion of H_2O in granitic liquids: I. Experimental data; II. Mass transfer in magma chambers. *In:* Geochemical Transport and Kinetics. Hofmann AW, Giletti BJ, Yoder HS, Yund RA (eds) Carnegie Inst. Washington Publ., Washington, DC, pp 139-170

Shishkina TA, Botcharnikov RE, Holtz F, Almeev RR, Portnyagin MV (2010) Solubility of H_2O- and CO_2-bearing fluids in tholeiitic basalts at pressures up to 500 MPa. Chem Geol 277:115-125

Sierralta M, Nowak M, Keppler H (2002) The influence of bulk composition on the diffusivity of carbon dioxide in Na aluminosilicate melts. Am Mineral 87:1710-1716

Spickenbom K, Sierralta M, Nowak M (2010) Carbon dioxide and argon diffusion in silicate melts: insights into the CO_2 speciation in magmas. Geochim Cosmochim Acta 74:6541-6564

Stanley BD, Hirschmann MM, Withers AC (2011) CO_2 solubility in Martian basalts and Martian atmospheric evolution. Geochim Cosmochim Acta 75:5987-6003

Stolper EM, Fine G, Johnson T, Newman S (1987) Solubility of carbon dioxide in albitic melt. Am Mineral 72:1071-1085

Stolper EM, Holloway JR (1988) Experimental determination of the solubility of carbon dioxide in molten basalt at low pressure. Earth Planet Sci Lett 87:397-408

Tamic N, Behrens H, Holtz F (2001) The solubility of H_2O and CO_2 in rhyolitic melts in equilibrium with a mixed CO_2-H_2O fluid phase. Chem Geol 174:333-347

Taylor WR (1990) The dissolution mechanism of CO_2 in aluminosilicate melts - infrared spectroscopic constraints on the cationic environment of dissolved $[CO_3]^{2-}$. Eur J Mineral 2:547-563

Thibault Y, Holloway JR (1994) Solubility of CO_2 in a Ca-rich leucitite: effects of pressure, temperature, and oxygen fugacity. Contrib Mineral Petrol 116:216-224

Tingle TN, Aines RD (1988) Beta track autoradiography and infrared spectroscopy bearing on the solubility of CO_2 in albite melt at 2 GPa and 1450 °C. Contrib Mineral Petrol 100:222-225

Tossell JA (1995) Calculation of the ^{13}C NMR shieldings of the CO_2 complexes of aluminosilicates. Geochim Cosmochim Acta 59: 1299-1305

Vetere F, Botcharnikov RE, Holtz F, Behrens H, de Rosa R (2011) Solubility of H_2O and CO_2 in shoshonitic melts at 1250 °C and pressures from 50 to 400 MPa: implications for Campi Flegrei magmatic systems. J Volcanol Geotherm Res 202:251-261

Watson EB (1991) Diffusion of dissolved CO_2 and Cl in hydrous silicic to intermediate magmas. Geochim Cosmochim Acta 55:1897-1902

Watson EB, Sneeringer MA, Ross A (1982) Diffusion of dissolved carbonate in magmas: experimental results and applications. Earth Planet Sci Lett 61:346-358

Webster JD, Goldoff B, Shimizu N (2011) C-O-H-S fluids and granitic magma: how S partitions and modifies CO_2 concentrations of fluid-saturated felsic melt at 200 MPa. Contrib Mineral Petrol 162:849-865

White BS, Montana A (1990) The effect of H_2O and CO_2 on the viscosity of sanidine liquid at high pressures. J Geophys Res 95:15683-15693

White WB (1974) The carbonate minerals. *In:* The Infrared Spectra of Minerals. Farmer VC (ed) Mineralogical Society, London, p 227-284

Wood BJ, Bryndzia LT, Johnson KE (1990) Mantle oxidation state and its relationship to tectonic environment and fluid speciation. Science 248:337-345

Wyllie PJ, Tuttle OF (1959) Effect of carbon dioxide on the melting of granite and feldspars. Am J Sci 257:648-655

Zhang C, Duan Z (2010) GFluid: an Excel spreadsheet for investigating C-O-H fluid composition under high temperatures and pressures. Computat Geosci 36:569-572

Zhang Y, Ni H (2010) Diffusion of H, C, and O components in silicate melts. Rev Mineral Geochem 72:171-225

Zhang Y, Stolper EM (1991) Water diffusion in a basaltic melt. Nature 351:306-309

Zhang Y, Xu Z, Zhu M, Wang H (2007) Silicate melt properties and volcanic eruptions. Rev Geophys 45:RG4004, doi:10.1029/2006RG000216